A Hybrid Lagrangian-Eulerian Solver for Non-Newtonian Arterial Flow with Vessel Compliance

Akram Elsayed & Ahmed Elsayed

Table of Contents

Summary

Cardiovascular disease remains the leading cause of global mortality, and while current clinical tools offer valuable information needed in their diagnosis, they predominantly assess arterial risk through structural behaviour rather than hemodynamic criteria. This project aims to develop a hybrid computational fluid dynamics solver by coupling the Lattice Boltzmann Method (LBM), Smoothed Particle Hydrodynamics (SPH), and a three element Windkessel lumped parameter model to simulate non-Newtonian blood flow in compliant arterial geometries. The solver is to be validated against analytical methods (such as Poiseuille flow) and complex emergent behaviour (such as the Von Karman vortex), all while being applied to fictional, yet clinically plausible case studies, one of which being a 74.6% carotid artery stenosis case. The solver was able to produce accurate and physical results for the fictional case studies (e.g. peak velocity amplification of 17.4x, maximum wall shear stress of 30.36 Pa, and a trans-stenotic pressure drop of 35.78 mmHg; all are consistent with clinical thresholds). While the solver proved to be accurate and viable as it is, it is limited by its 2D nature, the use of linear spring compliance for the vessel walls, and the Windkessel pressure clamping, each of which were addressed accordingly..

Introduction

Cardiovascular diseases (CVDs) are the leading cause of mortality globally, accounting for an estimated 19.8 million deaths in 2022 (“Cardiovascular diseases (CVDs),” n.d.) . While clinical risk assessments traditionally focus on lifestyle factors and structural imaging, such as arterial calcium (AC) cans, these methods often overlook the dynamic hemodynamic behaviour of blood flow. Pathologies such as atherosclerosis manifest as lipid rich plaque that narrows the vessel’s lumen (stenosis), altering the flow’s laminarity and wall shear stress.

This project proposes that blood flow analysis can lead to more predictive physiological assessment than structural data alone. However, accurately simulating the arterial environment requires accounting for two factors; non-Newtonian fluid behaviour and vessel wall compliance. Current models often choose between computational efficiency that is needed for complex geometries with the high fidelity needed for fluid-structure interactions (FSI).

As such, this project develops a coupled computational model. The system uses the Lattice Boltzmann Method (LBM) to model the non-Newtonian behaviour of blood via the Carreau-Yasuda viscosity model. Simultaneously, Smoothed Particle Hydrodynamics (SPH) is used to also run a fluid simulation while quantifying vessel wall compliance, integrated with a Windkessel model to simulate the expansion and recoil of elastic arteries. Both models will average their pressure fields and final velocity/pressure boundary conditions will be fed into a systematic Windkessel model to calculate the change in blood in terms of physiologically realistic pressure. This is done using resistance-compliance dynamics, with this pressure being fed back as an outlet boundary condition to close the circulatory loop.

By coupling these methods, the solver would provide a high fidelity tool for mathematically quantifying hemodynamic stress, offering the possible potential for cardiovascular research and educational screening.

The key point of using a computational fluid solver isn’t just for academic purposes. Most standard screening methods, such as CT scans, angiograms, Doppler ultrasound, etc., carry limitations (being static structural snapshots in nature, highly invasive procedures, and being expensive, as examples); a fluid solver capable of deriving wall shear stress, pressure gradients, and vessel wall compliance just from a single patient’s vessel geometry would prove to be an immense advancement in non-invasive risk assessment (given it is set up correctly and is sufficiently advanced as a method). Using a fluid solver, however, is set back by its inherent limitations (validation, computational cost, accurate model assumptions), but our goal here isn’t to replace clinical measurements with computational solvers, but to provide another layer of insight that structural imaging alone cannot offer.

Literature Review

The review will begin with an overview of arterial structure and pathophysiology, followed by hemodynamic principles and modelling approaches.

The arterial system is rather a difficult system to simulate, due to its branching complex geometry and the physiological structures of the cardiovascular system.

The Arterial System

Vascular Structure and Physiologically

The vascular system is the transport median of blood within the cardiovascular system. It is made up of systemic and pulmonary circuits, which are made up of arteries, arterioles, capillaries, venules, and veins.

Systemic circuits contain the majority of arteries. There are two types of such, systemic arteries that contain oxygenated blood to all tissues, and systemic veins containing de-oxygenated blood that returns back to the heart. On the other hand, the pulmonary circuit is the opposite, where pulmonary arteries move de-oxygenated blood to the lungs and pulmonary veins transport oxygenated blood to the heart to repeat the cardiac cycle.

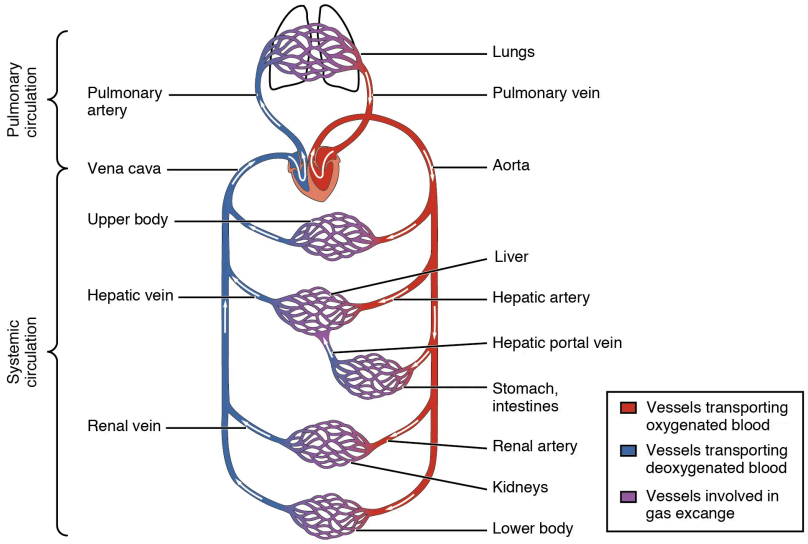

Systematic blood circuit figure

Although there is physiological difference in such vessels, the anatomy of all blood vessels are the same. All vessels have three layers as the following:

- **Tunica Intima**: the inner most tunic is made up from simple squamous endothelium, a basement membrane, and a thin layer of areolar connective elastic tissue. Larger arteries tend to have an internal elastic membrane between the tunica intima and tunica media.

- **Tunica Media**: The tunica media is in the middle between the intima and externa. It is the thickest layer in arteries and contains smooth muscles which makes it the layer that contracts and dilates to move blood through the peripherals of the body back to the heart.

- **Tunica Externa**: Is the outermost layer of blood vessels and acts as a support layer of collagenous fibers, some elastic fibers, and in veins, groups of smooth muscle fibers to push up the blood. In arteries the tunic externa tends to be thinner than the tunica media.

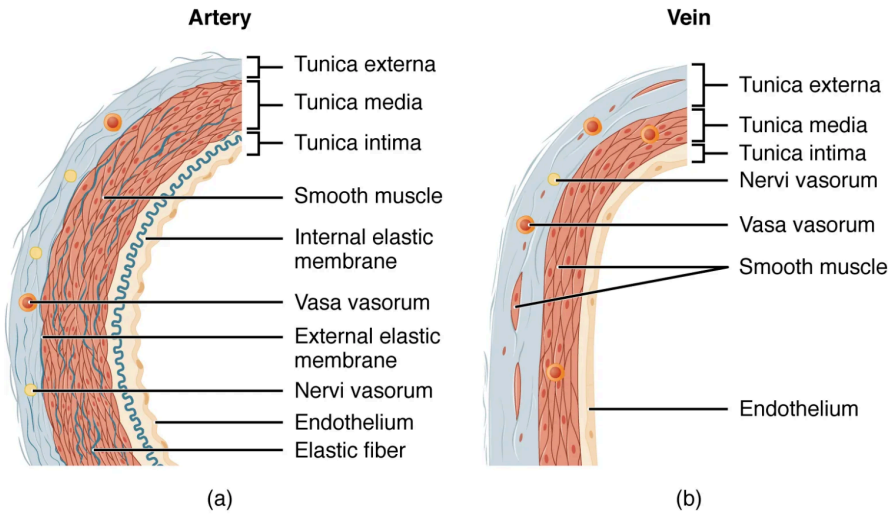

Layers of a blood vessel figure

Arterial Structural and Elastic Behaviour

Arteries near the heart are called **“elastic arteries”**, with a diameter greater than 10 millimeters in healthy adults and the walls tend to be mainly made up of elastic fibers, allowing it to expand in diameter due to ventricular ejection and recoil to maintain pressure which are both mechanics we have to consider in the simulations.

As arteries move farther from the heart, the diameters decrease, with “muscular arteries” that range from 0.1mm to 10, allowing for vasoconstriction for blood movement and distribution. The elasticity of peripheral vessels in comparison to thoracic vessels or other major vessels decreases, as such there is a decrease in pressure.

Arterioles’ lumen average at 30 micrometers or less, with some being big enough for 1 RBC at a time, as they contain one or two smooth muscle layers and thin tunica externa as a primary resistance vessel to control blood flow and pressure.

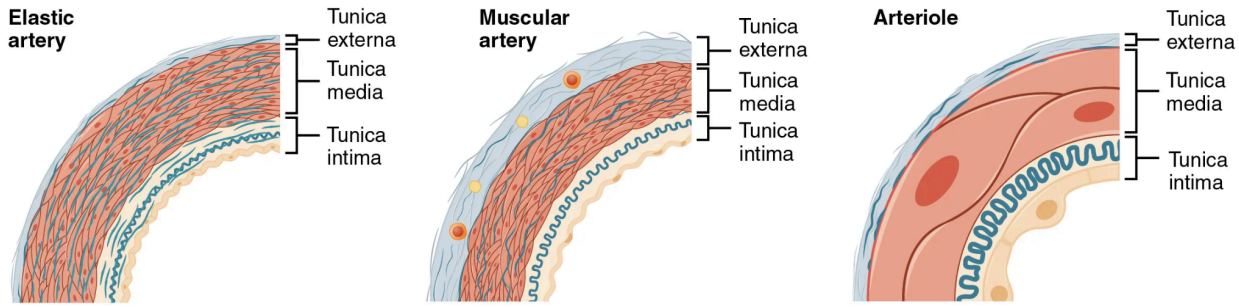

Arteries types figure

Vascular Pathophysiology and Diseases

Having studied a background of the structure, physical and physiological, composition, and hemodynamics of the cardiovascular system, it is important for the project to research how

physiological changes can reflect this rather complex process. Vascular pathophysiology is the study of any structural changes, biochemical imbalances, and mechanical stresses within blood vessels.

This project specifically, arterial pathology; arterial pathology is the leading cause of mortality in many countries, especially Western countries, with atherosclerosis being the leading cause (P et al., 2019) .

Atherosclerosis

Atherosclerosis refers to the general stiffening and hardening of arteries starting during childhood and teenage years, and progresses till commonly 40s - 50s where most symptoms onset. It begins with fatty streaks, where plasma lipids accumulate inside macrophages, forming “foam cells”. As these cells die, extracellular lipids can provoke inflammation and fibrosis, producing palpable plaque as seen in large and medium arteries. As plaques enlarge, they may calcify or ulcerate, creating a surface thrombus.

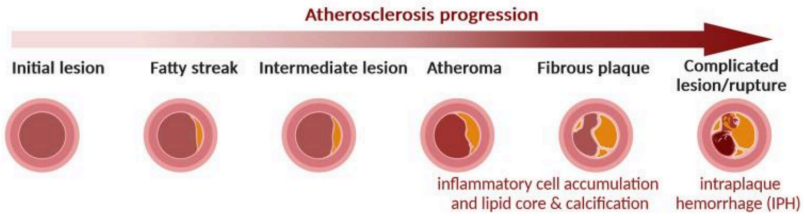

Atherosclerosis progression figure

Plaque rupture or thrombosis may narrow or occlude arteries, resulting in cerebral, mesenteric, coronary, or renal ischaemia. Conversely, plaques can embolize fatty debris or cholesterol crystals, causing an “athero-embolism” to the legs, kidneys, etc. While often subclinical, they can occasionally lead to renal failure, malignant hypertension, or cerebrovascular accidents (CVA) like a shooting embolism .

	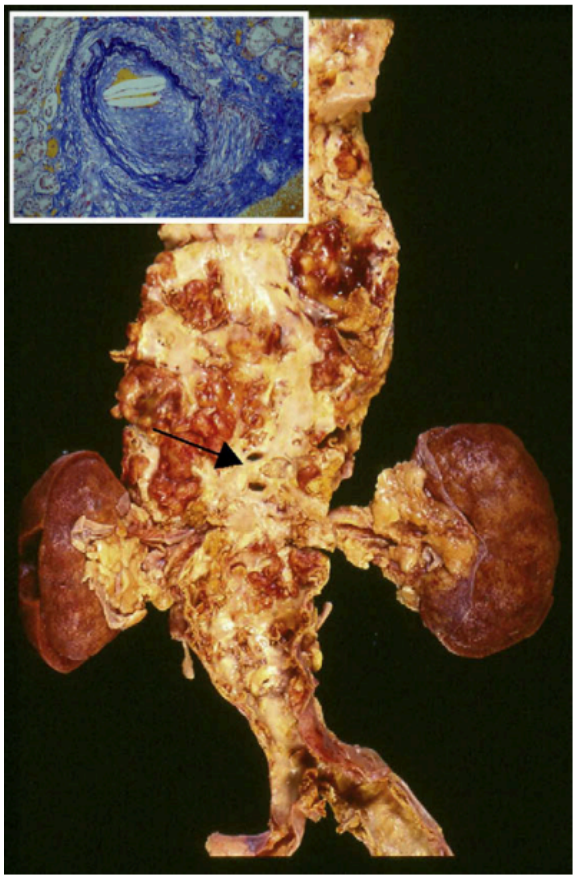
Moderate atheroma of the abdominal aorta with fibrous plaques, with branching ostial stenosis figure	Severe atheroma at the aorta with plaque ulceration, thrombus formation, and embolic damage to the renal arteries figure

Plaque distribution can impact haemodynamic stress, particularly at bifurcation and curvature points, where turbulent flow or disturbed shear stress can change how the endothelial-related gene expresses itself and promote lipid retention and inflammation

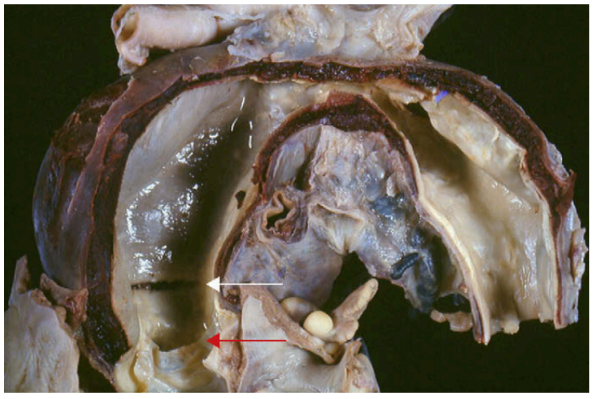	Thoracic aortic stenosis (coarctation) at a curvature point (aortic arch). A typical transverse intimal tear (white arrow), and an extensive dissection along the aortic arch (red arrow) figure

	45-year-old woman with renal artery stenosis due to multiple transverse fibromuscular ridges of fibromuscular dysplasia figure

Hemodynamic Factors

Hemodynamic forces, particularly wall shear stress (WSS), are the main factors in the development of these conditions, given they are linked to the start of and progression of cardiovascular diseases, such as atherosclerosis and stenosis. WSS is defined as the tangential force per unit area exerted by flowing fluid on a surface.

$$\tau_{\omega} = \mu\, du/dy\,;\;\; y = 0$$

(e.q. 1)

Where μ is the dynamic viscosity of blood and du/dy is the velocity gradient at the vessel wall. In healthy arteries, blood is mainly laminar, and the relationship between pressure drop, flow rate, and vessel geometry is described using Hagen's law.

$$\Delta P = \frac{8\mu LQ}{\pi r^4}$$

(e.q. 2)

The pressure drop ΔP drop in a vessel length of L and radius r, for a volumetric flow rate Q. The Hagen law shows that a small difference in vessel radius due to stenosis, will dramatically increase the resistance, in turn changing the WSS value. This equation is, in simple terms, the definition of how the vessel radius is proportional to the flow r^4. Any small change in the vessel diameter, such as that caused by atherosclerotic plaque, will have effects on flow and shear stress.

The general nature of a flow regime, whether laminar or turbulent, can be quantified using the Reynolds equation.

$$Re = \frac{\rho VD}{\mu}$$

(e.q. 3)

Where:
Re is the Reynolds number

ρ is the density of the fluid
V is the mean velocity
D is the diameter of the pipe (this case, vessel)
μ is the dynamic viscosity

The Reynolds number describes how ordered the fluid is flowing; larger Re values describe turbulent flow and lower ones describe laminar flow. It is often around a range that describes these behaviours, with laminar flow being represented as Re < 2300 and turbulent flow being represented as Re > 2900.

In stenotic regions, the Reynold's number may rise and the flow can become disturbed or transitional. This leads to abnormal "shear flow" at the region, and therefore may cause issues, such as endothelial dysfunction, inflammatory cell recruitment, and/or atherosclerotic plaque formation. Tracking this value will be deemed as one of the main "warning signs" to see if the region is healthy or not, and how it may damage the local area with high Re values.

Arterial Flow Models

Arterial Flow Modelling

To properly map out how the blood should act at arteries, specific simulations of the arterial tree are used. These should not be treated like a normal CFD simulation, however. There are 3 main ways to simulate as follows:

- **A 0D Windkessel Model**, where blood is treated as an electrical circuit, made up of resistors, capacitors, and inductors. This model works as the relationship between pressure and flow without considering vessel geometry, making it very fast to compute, and could be used in two main cases. 1) To calculate the global blood pressure and cardiac output. 2) Calculate the afterload and preload effects of blood, meaning after and before entering a vessel. (Van De Vosse and Stergiopulos, 2011).

- **1D Wave Propagation Model** is a model where the flow of blood is calculated using simplified Navier-Stokes equations over the cross-section of vessels, over and over, simulating different sections of the vessel and calculating the flow of the entire vessel or arterial tree. This model can be used to calculate and visualize pulse wave propagation, pressure waves, and can include the elasticity and recoiling effects of arteries, and most importantly, it can include patient-specific vessel geometry. While the Navier-Stokes equations themselves are general, many reduced 1D equations assume Newtonian viscosity for mathematical simplicity, though non-Newtonian versions exist (Van De Vosse and Stergiopulos, 2011).

- **3D/2D Computational Fluid Dynamics** uses different models, such as the Finite Volume Method (FVM), Lattice Boltzmann Method (LBM), and Smoothed Particle Hydrodynamics (SPH), which are all governed by the full Navier-Stokes equations, making the most realistic flow and geometry-wise. It can compute wall shear stress, flow vortices (dissections), secondary flow, disturbance, turbulence increase, etc. This model can be used for atherosclerosis, aneurysms, other stenosis-related diseases, bifurcation points, and so on. The main downside is how computationally and technically heavy it is to produce (Van De Vosse and Stergiopulos, 2011).

Those models can be coupled with each other to compensate for their shortcomings. Such are the following examples are:

- 0D Heart and a 1D arterial tree, which means the heart can be treated as a lumped parameter and the major arteries as cross-sectional 1D geometries. The heart is modelled as pressure-volume elements, making it a 2-element Windkessel model (resistance, compliance, valves), and the values outputted from the heart model are the 1D equations

Model	Comparison
OD	The fluid is collapsed into zero dimensions and only considered to be an “electrical circuit”, such being described in terms of Ohm’s law (resistance, voltage, and current). No geometry is involved.
1D	A simplified Navier-Stokes equation is used to work through a cross-section of a vessel(s). Each iteration of the simulation, you work through a different slice of the vessel/arterial tree. The model is used to calculate and visualize wave propagation, pressure waves, and may also include the elasticity of the vessel walls and recoiling effect of the arteries.
2D/3D	“Speacialized” models are to be used in this context; finite volume method, Lattice Boltzmann Method, and Smoothed Particle Hydrodynamics are used, such all being governed by the full Navier-Stokes equations, thus providing the greatest accuracy. Wall shear stress, flow vortices, secondary flow, disturbance, turbulence increases, and so on can all be computed.

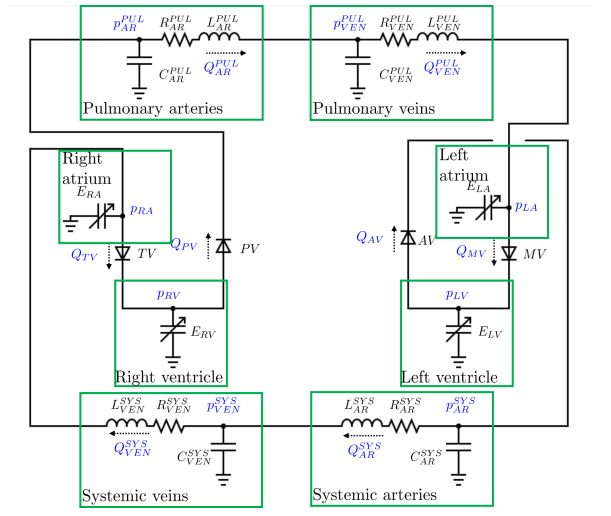

Lumped Parameter Cardiovascular Model (Formaggia et al., 2010)

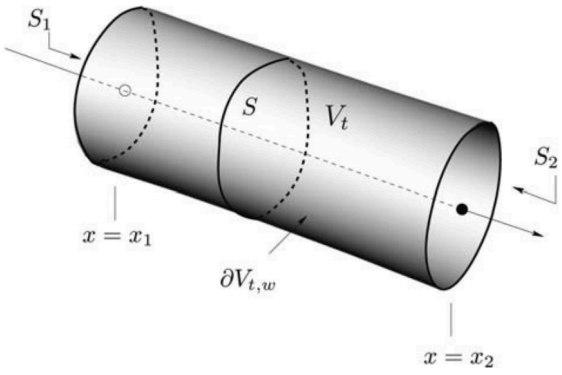

1D Cross-sectional pipe example (Formaggia et al., 2010)

Up to this point, using an LBM only method might seem to be better over the hybrid approach. This is actually countered by the fact that SPH is capable of filling in the voids that come with using LBM as a fluid method; LBM is fundamentally an Eulerian method, which are notorious for struggling with major boundary deformations (conversely, this is characteristic of blood vessels with the physical expansion and recoil of elastic arteries under pulsatile pressure), making it difficult to encode in a static lattice without constant mesh-updates, increasing computational cost. SPH circumvents this by acting on a Lagrangian frame, handling moving boundaries with each since you can describe the vessel walls in terms of special particles whilst incorporating a spring restoring force. This justifies the coupling of the methods, as each one compensates for the shortcomings of the other. Even this, however, can be countered by noting that Arbitrary Lagrangian-Eulerian (ALE) methods in finite volume codes achieve the same goal more efficiently. This is true in its own right, but ALE implementations are significantly more complex (notably, with the mesh-deformation algorithms that come with the method). The LBM-SPH coupling works as a balanced point; it is good enough to fulfill the required precision and cheap enough that we can run it viably using our relatively weak hardware.

Fluid Rheology

Viscosity Models

Unlike most fluids, blood is **non-Newtonian**, meaning its viscosity is variable against the force applied (more specifically, the shear rate $\dot{\gamma}$ in $\frac{1}{s}$ or s^{-1}). Among the most common models, two stand out: The **Power Law** model and the **Carreau(-Yasuda) constituent flow** model (Pedro Vayssiere Brandao et al., 2004) . The power law model is a simplified form of calculating the **apparent viscosity** η_a for any given fluid. Mathematically, it is expressed as:

$$\eta_a = k\dot{\gamma}^{n-1}$$

(e.q. 4), (Chandler, 2019)

Where η_a is the apparent viscosity, k is the **consistency index** (how thick the fluid at a shear rate of 1), and n is the **behaviour index** (how the fluid behaves; if $n < 1$, shear thinning; if $n = 1$; Newtonian if $n > 1$, shear thickening).

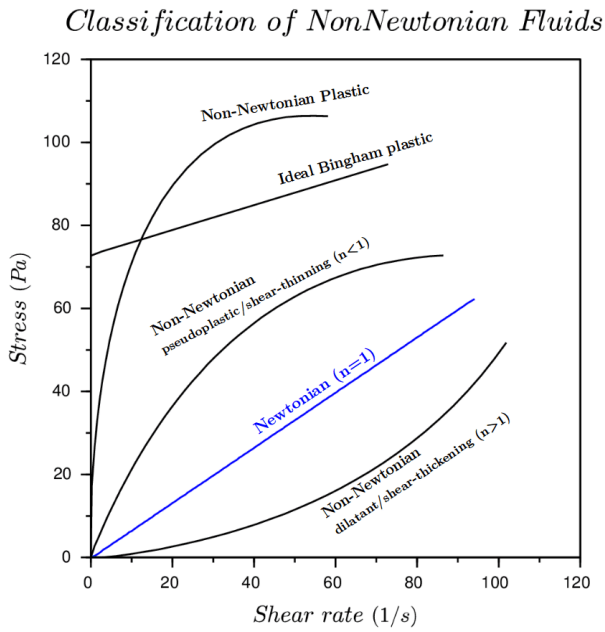

("Non-Newtonian Models | Materials," n.d.) figure

In ordinary contexts, k is defined as:

$$k = \eta_0 \lambda^{-2p}$$

(e.q. 5)

Where η_0 is the **low shear rate newtonian plateau viscosity** (will be explained in a moment) λ is a **time parameter** (is used to make the total value of the equation dimensionless), and p is a **dimensionless parameter** related to the slope that will be graphed in the apparent viscosity-shear rate graph.

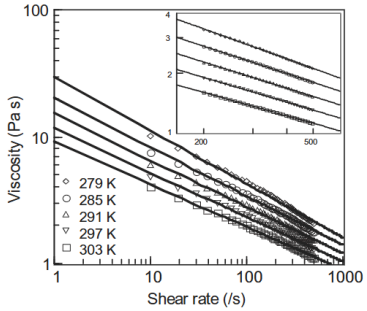

Figure 1. Viscosity–shear rate curves at several temperatures for a 10% aqueous solution of CMC. Although curves are approximately linear over the shear range 10–500/s, fully developed power-law behavior only occurs at rates above about 200/s as illustrated in the inset.

(Chandler, 2019) figure

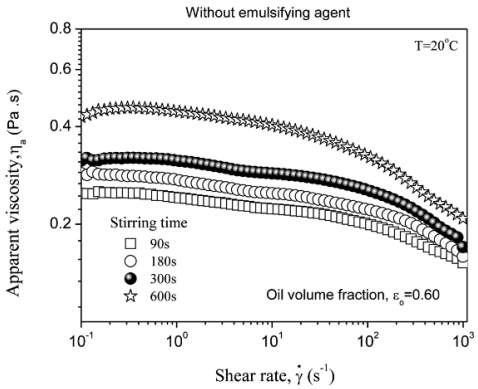

FIG. 12. Apparent viscosity at a function of shear rate with 0.6 oil volume fraction under different stirring time.

(Zhang et al., 2013) figure

However, the power law's viability breaks down at lower shear rates (general example: $0 < \dot{\gamma} < 1$ power law is invalid). For that, we can use the **Carreau constituent flow equation**, which works at the **low shear rate newtonian plateaus**, which are the initial regions on an apparent viscosity-shear rate graph where the fluid would act like a normal newtonian fluid at low shear rates:

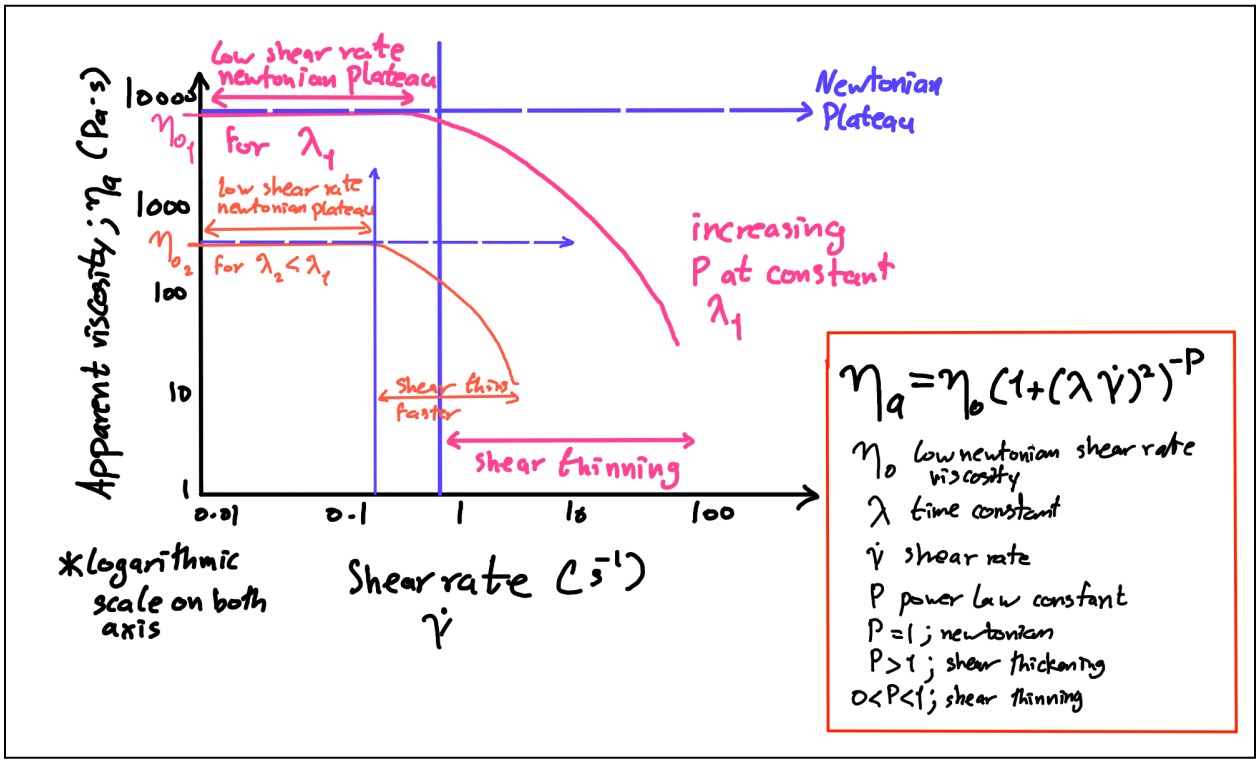

This graph describes the typical Carreau fluid for power law constants of $0 < p < 1$, allowing for shear thinning behaviour to be obtained. An example of this would be ketchup being squeezed out of the bottle, which increases the shear rate on the fluid, thereby reducing the apparent viscosity accordingly.

Going back to the λ parameter, it might seem a bit "off" in the sense that it only represents time. However, if it weren't for it, the units would mismatch with that of viscosity, becoming $\frac{Pa}{s}$ instead of the usual units. In other words, it "counteracts" the units of shear rate, them being s^{-1}. That's mathematically only, but in a physical sense, it describes how fast the fluid will start behaving non-Newtonian (in the graph above, the second origin line has a lower λ slope and η_0 values, making the fluid start with a lower "initial viscosity" and start its non-Newtonian behaviour sooner than the first fluid.)

However, for a more flexible method than the Carreau constituent flow equation, the Carreau-Yasuda constituent flow equation is utilized, as it captures both high and low shear rate Newtonian plateau. Mathematically, it is expressed as:

$$\frac{\eta_a - \eta_\infty}{\eta_0 - \eta_\infty} = (1 + (\lambda\dot{\gamma})^a)^{\frac{m-1}{a}},$$

(e.q. 6)

Where η_∞ is the infinite shear rate viscosity (in effect, the absolute lowest viscosity at the highest possible shear rate for this fluid), a is a transition parameter, easing the shift from the low shear rate newtonian plateau into the non-newtonian behaviour, and m is another power law constant (not to be confused with the aforementioned two before this; they are all unique from each other). The graph plotted by the Carreau-Yasuda equation is usually:

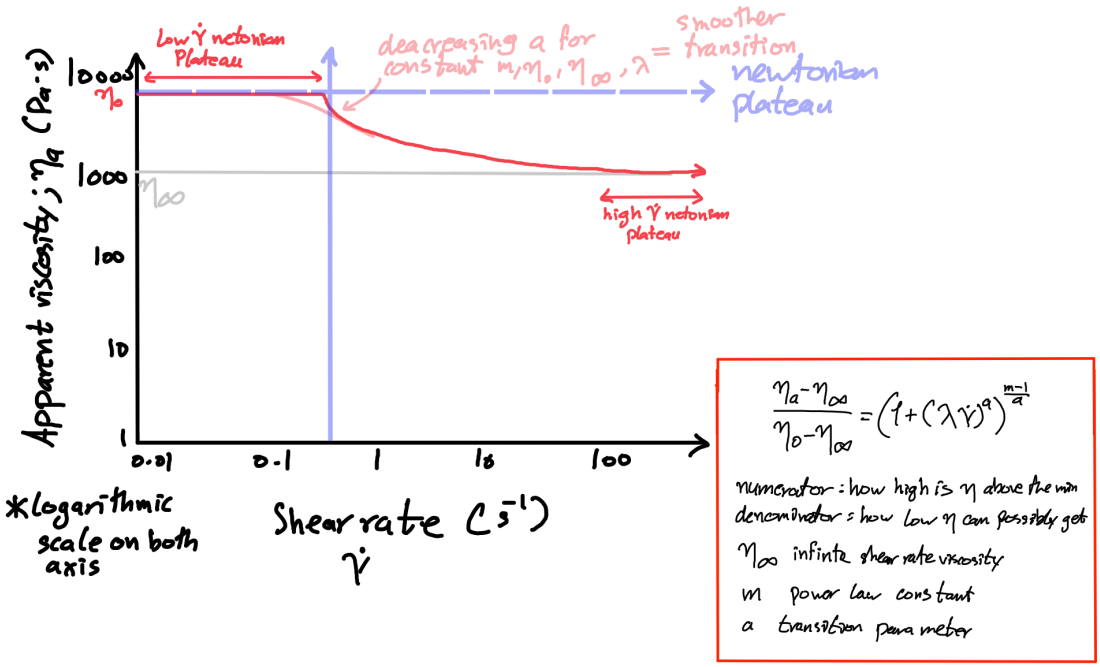

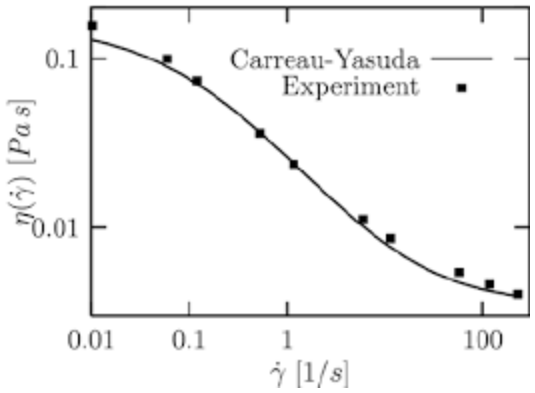

Unlike the previous model, the Yasuda variant can express a second Newtonian plateau, such being at the high shear rate as the fluid reaches the “maximum viscosity change” for the given material. In summary, due to the breakdown of the power law model at low shear rates, the Carreau-Yasuda model will be selected for the solver, as it can capture both low and high Newtonian plateaus that are relevant to arterial flow.

Womersley’s Number

For unsteady flows (such as blood), it is hard to universally solve them without making “custom-built systems” for every example. For that, some dimensionless parameters were made to ease the solving for these fluid flows. A major example would be **Womersley’s Number** (Jr, 1955), (W_0 or α), a “general-purpose indicator of the nature of unsteady flow”. Mathematically, it is expressed as:

$$W_0 = \frac{L}{2}\sqrt{\frac{n}{v}},$$

(e.q. 7)

Where L is a characteristic length (for a cylinder/cylinder-like structure) of the studied area in metres, n is the frequency of the unsteady flow in radians/s, described as $n = 2\pi f$ (f is the frequency in cycles/s), and v is the **kinematic viscosity** of the fluid in m^2/s.

How the Womersley’s number describes behaviour is typically in ranges of values:

$$W_0 < 1;\ quasi\ steady$$

$$W_0 > 1;\ deviates\ from\ quasi\ steady$$

Where “quasi steady” means that at any time, the instantaneous flow rate is determined by the instantaneous pressure gradient (Loudon and Tordesillas, 1998). However, because of the otherwise significant size differences between the aorta and the fine capillaries (3 orders of magnitude), a slightly different equation is used for human blood:

$$W_0 = L\left(\frac{\omega\rho}{\mu}\right)^2,$$

(e.q. 8)

Where ω is the **angular frequency** in radians/s, ρ is the **density** of the fluid kg/m^3, and μ is the **dynamic viscosity** in Pa·s.

Development/Analysis

Upon setting up the general research for the project, we can move on to the development section. Here, our main goal is to set up and create a fluid solver for cardiac environments, using a variety of governing equations and methods. To set up the project's beginning, we start by a development plan based on important milestones and estimations for how long they will take.

Name	**Date**
Review of past models & solvers	5-10/01/2026
Buffer day	11/01/2026
Brainstorm, research, and specify solver specifications and features	12-16/01/2026
Buffer	17/01/2026
Basic 2D Pipe Arterial Model	18-24/01/2026
Buffer	25/01/2026
LBM Solver version	26/01/2026 - 03/02/2026
SPH Solver version	26/01/2026 - 03/02/2026
Buffer	04/02/2026
Import Medical imaging geometry	05/02/2026 - 10/02/2026
Buffer	11/02/2026
Hemodynamic Testing	12/02/2026 - 24/02/2026
Buffer	25/02/2026
Comparative analysis of solvers and literature	26/02/2026 - 04/03/2026
Buffer	05/03/2026
Optimization of models	06/03/2026 - 09/03/2026
Buffer	10/03/2026
Draft of Essay	11/03/2026 -

Methodology and Key Model

Governing Equations

Fluid flow in arteries can be described using Eulerian or Lagrangian specifications. Eulerian methods focus on a fixed spatial point and are used the most in arterial CFD; some examples are the Finite Volume Method and Lattice Boltzmann Method. While Lagrangian methods track a fluid as a particle, making it useful for particle-based simulations with large deformations and moving boundaries.

Eulerian Fluid Specification

Of the two baseline methods of fluid modelling, **Eulerian Fluid Modelling** views fluid flow from the perspective of a “universal grid”; you divide a space into a grid where you apply and track fluid behaviour across the divided area as the fluid flows through it. This grid is called the **Eulerian field**. The field is represented as a function of position (x) and time (t). For example, the velocity field is defined as:

$$u(x,t)$$

Now, suppose we have this fluid field u, and another generic field with Eulerian specification of F(x,t). You may need to know about the total rate of change of this field F experienced by a specific fluid parcel moving through the flow. This is computed by the (1D) material derivative, defined as:

$$\frac{DF}{Dt} = \frac{\partial F}{\partial t} + (u \cdot \nabla)F$$

(e.q. 9)

This expression tells us the total rate of change of a field F experienced by a moving fluid parcel is equal to the sum of:

- The local rate of change $\frac{\partial F}{\partial t}$ represents how the field changes at a fixed location in space.
- The convective rate of change $(u \cdot \nabla)F$ represents how the fluid changes because the parcel moves through spatial variations in the field.

Now, the main Euler fluid flow equations that will be used here are:

$$\frac{D\rho}{Dt} = -\ \rho\nabla \cdot u$$
$$\frac{Du}{Dt} = -\frac{\nabla p}{\rho} + g$$

(e.q. 10, 11)

For:

ρ is the density of the fluid
u is the flow velocity
p is the pressure (in this context, the pressure gradient)

For inviscid fluid flow (zero or insignificant viscosities), there is a form of the Eulerian equations that governs this. It is described as:

$$\rho \frac{Dv}{Dt} = -\nabla p + \rho g$$

(e.q. 12)

This form also relates the pressure gradient to the acceleration (in the form of the material derivative, that is), so crossing specific interactions with each other becomes easier.

Lagrangian Fluid Specification

The other baseline method of fluid modelling (the first being **Eulerian Fluid Flow**) is **Lagrangian Fluid Modelling**, which views fluid flow from the perspective of **individual fluid particles**, instead of being tied to a "global" grid as in the Eulerian system.

Every particle is labelled with an initial position, x_0, at some reference time t_0. As the fluid moves, the same particle would occupy a new position $X(x_0, t)$ at time t. Mathematically, this is represented as:

$$X : (x_0, t) \rightarrow X(x_1, t)$$

(e.q. 13)

This specifies the trajectory or pathline of the fluid parcel (the fluid parcel is an arbitrary unit/collection) in space and time. In other words, it provides us with the position of the fluid parcel at any given time. And because this is a function that provides us with the position, taking its derivative will give us the parcel's velocity:

$$u(x_0, t) = \frac{\partial X(x_0, t)}{\partial t},$$

(e.q. 14)

The Lagrangian method is not fixed or relying on a grid to dictate its flow and position ("it doesn't concern itself with what happens at a stationary position"). Instead, it tracks how a single, identifiable element (the fluid parcel) in the continuum evolves in respect of time (its mass, density, momentum, velocity, etc.).

One analogy that can help with understanding is "tagging one droplet of colour in a current, and seeing how its position and any property it may carry (e.g., temperature, concentration, density, etc.) changes according to the recent local history it experiences".

Finally, we can denote one scalar (mass, temperature, etc.) or vector (divergence, curl, etc.) property using F, the total rate of change of that property is written as the material derivative:

$$\frac{DF}{Dt}$$

(e.q. 15)

The derivative of F shows us how F changes as the particle moves, and not just with respect to time. In other words, these properties would change with respect to the local history experienced by the particle (hence providing an accurate answer). (Batchelor, 2010)

Navier-Stokes Equations

Before we can start progress on the fluid solvers, we need to cover the governing equations related to the fluid's motion. In simple words, they state what the fluid should and shouldn't do as it flows (e.g., density should be the same everywhere, no mass is created or lost, likewise with momentum and other properties, and much more). The governing equations for this context are the **Navier-Stokes equations** (or N-S equations/NSEs for short):

$$\frac{\partial u}{\partial t} = 0$$

$$\frac{\partial u}{\partial t} = \frac{1}{\rho}\frac{\partial p}{\partial x} + \nu\left(\frac{\partial^2 u}{\partial x^2}\right)$$

$$\frac{Du}{Dt} = -\frac{1}{\rho}\nabla p + \mu\nabla^2 u + g$$

The first equation describes incompressibility.
The second equation describes the momentum of the fluid in terms of density and pressure.
The last equation is the "typical" N-S form. It is the fluid equivalent of Newton's Second Law of Motion.

Numerical Solvers

Smoothed Particle Hydrodynamics (SPH)

SPH is a mesh-free, Lagrangian numerical method that offers many benefits, such as ease of setup in complex geometries due to it not relying on an appropriate mesh/grid to return accurate results. This makes the method well-suited for problems involving large deformations, moving boundaries/walls, and fluid-structure interactions. This perfectly describes the behaviour of arteries, making it great for macro-scale simulations.

Integral Interpolant and Discretized Summation

SPH is based on what is called an "integral interpolant", where you input discrete data points (the particles' positions, velocities, etc.) to output continuous values and ranges, as the fluid solvers assume continuous fields as a baseline for the calculations. Fundamentally, you can describe any property (e.g., velocity, pressure, viscosity, etc.) in the form of $f(r)$ in the following:

$$f(r) \approx \int_{\Omega} f(r_j) W(|r - r_j|, h)\, dr_j$$

This function uses the distance differences from the selected particle (usually denoted as r or r_i) from other particles (usually denoted as r_j or r'). This difference is used in a **smoothing kernel** that describes how much the particles should influence one another, with (a) closer particle(s) (i.e., smaller values from the subtraction) influencing one another the most.

This is the fundamental baseline of SPH numerically, but in terms of the simulation, you discretize it into a summation instead of an integral:

$$f(r) \approx \sum_j \frac{m_j}{\rho_j} f(r_j) W(|r - r_j|, h)$$

Now you work over all the particles in the domain and use the density (how close they are to one another in a select space) to apply whichever property at hand. The mass of each particle is just set to m = 1. This discretized form works as a weighted average of nearby particle values, with the kernel W working as the weight itself.

In simple words, we see how much nearby particles influence each other based on the kernel:

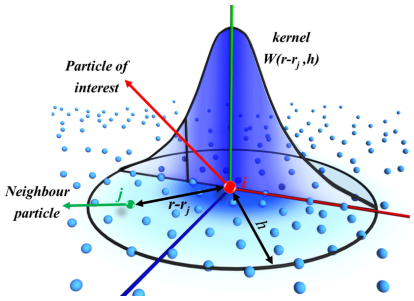

But the point here is that you substitute the $f(r)$ for any property with the appropriate terms to calculate it.

Systematic Pressure Gradient

The gradient form is used to know how certain properties are changing in space as the simulation evolves. For example, the pressure gradient shows us how the fluid is accelerating. Now, the naive form of this idea is:

$$\nabla \cdot f(r) \approx \sum_j \frac{m_j}{\rho_j} \cdot f(r_j) \cdot \nabla W(|r - r_j|, h)$$

However, this idea fails to conserve momentum:

For $i \leftarrow from\ j$: $f(r_j) \cdot \nabla W_{ij}$
For $j \leftarrow from\ i$: $f(r_i) \cdot \nabla W_{ij}$

However:

$\nabla W_{ji} = -\nabla W_{ij}$

These two gradients are opposite to one another, and to conserve mass, **these two gradients must equal one another**, hence this form is inappropriate for the context. To fix this, we use what is called a symmetric form:

$$f(r_i) \approx \rho_i \sum_j m_j \cdot \left(\frac{f(r_i)}{\rho_i^2} + \frac{f(r_j)}{\rho_j^2} \right) \cdot \nabla W_{ij}$$

Given the example of a pressure field, which is expressed using $F_i = -\frac{1}{\rho_i} \nabla P_i$, this reduces into:

$$P_i \approx -\sum_j m_j \cdot \left(\frac{P_i}{\rho_i^2} + \frac{P_j}{\rho_j^2} \right) \cdot \nabla W_{ij}$$

Now, the force particle i is experiencing from a specific particle j would be:

$$P_{\{i \leftarrow j\}} \approx -\sum_j m_j \cdot \left(\frac{P_i}{\rho_i^2} + \frac{P_j}{\rho_j^2} \right) \cdot \nabla W_{ij}$$

And the force particle j is experiencing from particle i would be:

$$P_{\{j \leftarrow i\}} \approx -\sum_i m_i \cdot \left(\frac{P_j}{\rho_j^2} + \frac{i}{\rho_i^2} \right) \cdot \nabla W_{ij}$$

But since $\nabla W_{ij} = -\nabla W_{ji}$:

$$P_{\{j \leftarrow i\}} \approx +\sum_i m_i \cdot \left(\frac{P_j}{\rho_j^2} + \frac{i}{\rho_i^2} \right) \cdot \nabla W_{ij}$$

For the conservation of momentum, we need $m_i \cdot F_{\{i \leftarrow j\}} + m_j \cdot F_{\{j \leftarrow i\}} = 0$, but since the previous equations tell us that the momentum of particle *i* is exactly equal to yet opposite to particle *j*, this perfectly satisfies the conservation of momentum, thus proving the symmetric form the best in this context.

Conservation of Properties

For any fluid solver to work, a continuity term/equation is required; the Lagrangian continuity is to be used, as the system is fundamentally discrete:

$$\frac{d\rho}{dt} = -\ \rho\nabla\ \cdot\ u$$

Further discretizing it for SPH application using the previous frameworks, we get:

$$\frac{d\rho_i}{dt} \approx -\ \rho_i \sum_j \frac{m_j}{\rho_j} \cdot \left(u_j - u_i\right) \cdot \nabla_i W_{ij}$$

$$\frac{d\rho_i}{dt} \approx \sum_j m_j \cdot \left(u_j - u_i\right) \cdot \nabla_i W_{ij}$$

Applying this globally in the system ensures the conservation of mass (i.e. nothing is created or destroyed, ensuring stability).

As of the conservation of momentum (physically), we can also use the Lagrangian form:

$$\frac{du}{dt} = \frac{1}{\rho}\nabla P\ +\ \nu\nabla^2 u\ +\ g$$

Discretizing for SPH again:

$$-\ \frac{1}{\rho_i}\nabla P_i \approx -\ \sum_j m_j \cdot \left(\frac{P_i}{\rho^2{}_i} + \frac{P_j}{\rho^2{}_j}\right) \cdot \nabla_i W_{ij}$$

Artificial Viscosity

However, SPH cannot conserve momentum properly if you apply this as it is. We require some form of artificial viscosity to prevent particle “interpenetration” (phasing through one another) and to properly capture shocks between particles. For this, we will use Monaghan’s artificial (Monaghan, 1992), viscosity, which states:

If $u_{ij} \cdot r_{ij} < 0$:

$$\Pi_{ij} = \frac{-\alpha\bar{c}_{ij}\mu_{ij} + \beta\mu^2{}_{ij}}{\rho_{ij}}$$

But if $u_{ij} \cdot r_{ij} > 0$:

$$\Pi_{ij} = 0$$

For μ_{ij} is:

$$\mu_{ij} = \frac{h\left(u_i - u_j\right) \cdot \left(r_i - r_j\right)}{\left|r_i - r_j\right|^2 + \epsilon h^2}$$

Where:

α and β are “tuning constants”. They “shift” their respective terms towards the desired outcome. α scales linearly while β scales quadratically with its terms. In practice, α acts as a “numerical thickness”, damping out small/unphysical behaviours, while β governs how hard the quadratic term acts like a “brake” for high-velocity collisions.
$\bar{c}_{ij}$ is the average speed of sound between particles i and j (in the simulation, an artificially high speed of sound is used to keep computation errors below 1%, so this check is required)
$\bar{\rho}_{ij}$ is the average density between particles i and j
u_{ij} is the relative viscosity between the particles
h is the smoothing length
ϵ is a safety factor. A small value.

In simple words, this artificial viscosity works by checking the difference between the relative positions of the particles and their relative velocities. You work out a “dot product” as it tells us if the particles are approaching one another (< 0) or "receding" from one another (> 0). Computationally, this is a relatively simple task.

Tait equation of State

SPH is fundamentally a “weakly compressible system”, and to circumvent this, we apply a pressure force depending on the density of particles; if the particles are clumped up (high density), we apply a pressure force so they move towards areas of lesser density, and if they are too spread out (low density), we apply a pressure force to pull them into areas of lower density.

To apply this, we use what is called the Tait equation of state (Robert H. Cole, 1948), (as a side note, this name is incorrect, as it is actually Cole's equation of state). In essence, we are relating pressure forces to density via:

$$P = B \cdot \left[\left(\frac{\rho}{\rho_0} \right)^{\gamma} - 1 \right]$$

For:
P is the pressure
B is a coefficient described as $B = \frac{\rho_0 c_0^2}{\gamma}$
c_o is an artificial speed of sound, usually expressed as $c_0 = 10 \cdot max(|u|)$, for max(|u|) is the “terminal velocity” of the fluid
γ is the polytropic exponent. In simple words, it describes how incompressible the fluid is; 7 is water-like, lower values make the fluid more gas-like, and higher values lead to more incompressible fluids. For blood flow, a value of 7 works well enough.
ρ is the current density, while ρ_0 is the “rest density” (usually 1)

Hybrid kernel (cubic spline + spiky)

Choosing the right kernel is important to provide accurate results and physical behaviours for the SPH solver. And after some research, we decided to use the cubic spline kernel:

$$W(q,h) = \alpha_d\{1 - \frac{3}{2}q^2 + \frac{3}{4}q^3,\ 0 \le q \le 1\}$$
$$W(q,h) = \alpha_d\{\frac{1}{4}(2 - q)^2,\ 1 \le q \le 2\}$$
$$W(q,h) = \alpha_d\{0,\ q \le 2\}$$

For:

q is a normalized distance, allowing for compact support. It is expressed as $q = \frac{|r - r_j|}{h}$.

α_d is a normalization constant. In 2D settings, it is expressed as $\alpha_d = \frac{10}{7\pi h^2}$.

The cubic spline method offers many benefits, such as acting smoothly up to the second derivative (I will get to that in a moment), providing compact support of 2h (hence only influences the relevant particles), and offering computational efficiency, as you are only computing polynomials (simple operations).

However, there is one point to be clarified on how these smoothing kernels work: The kernel itself works as a guide on how the particles should behave as they get closer and further, but in practice, the expressed behaviour in the simulation is the derivative of the graph.

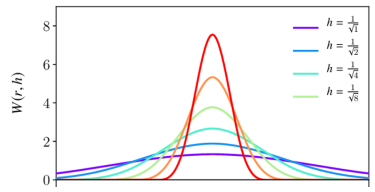	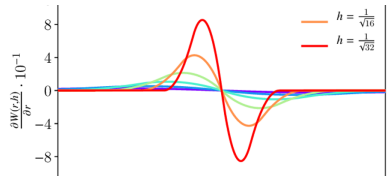	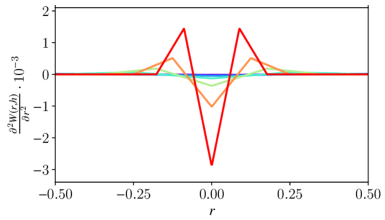
The Cubic Spline kernel graph	The first derivative: This is how the particles act in practice. As you can see, the force application significantly drops as you get closer to the “apex” of the original graph, up until there is no force applied, leading to clumping.	The second derivative

(Koschier et al., 2019)

Due to this, we cannot use a single kernel system, hence requiring a hybrid one. Further proving my point, this is how a single kernel system may look like (I experienced this whilst setting up the solver):

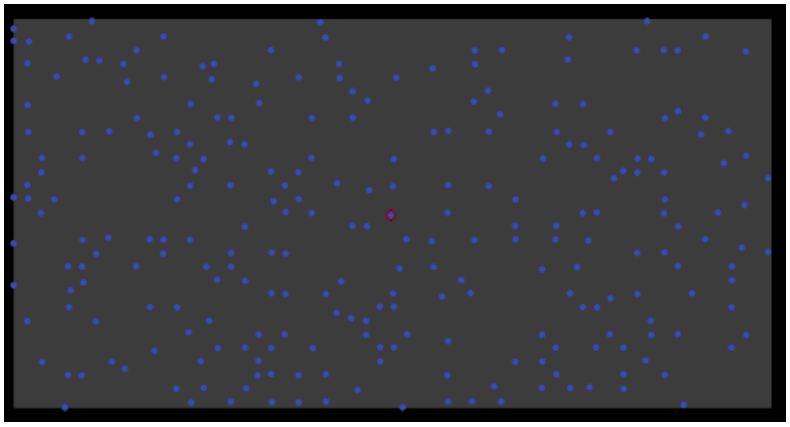

The particles are violently clumping together (there were also stability problems, further exasperating it).

To fix this, we will use another kernel known as “Spiky”, which is described as:

$$W(q,h) = \alpha_d \cdot \{(\frac{10}{\pi h^2}) \cdot (1-q)^3,\ 0 \le q \le 1\}$$

$$W(q,h) = \alpha_d \cdot \{0,\ q > 1\}$$

In practice (and the best way to explain this), the kernel looks like so:

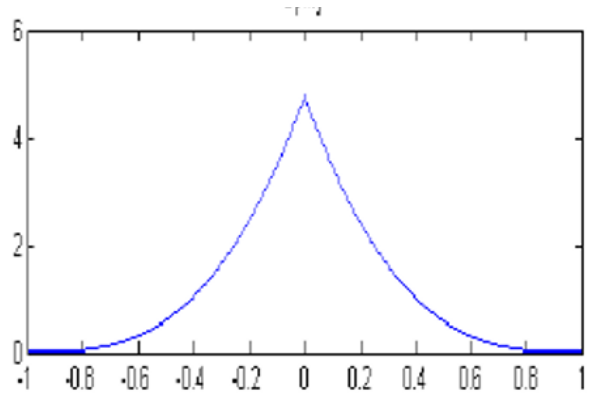	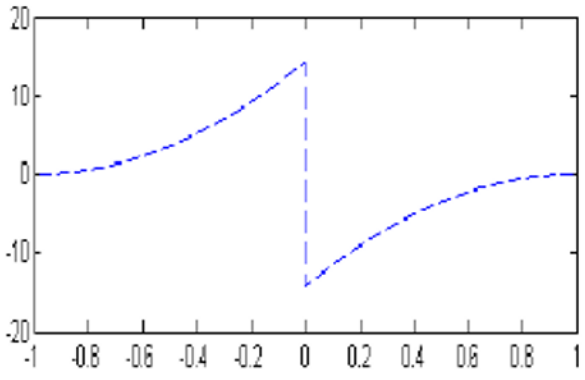
The typical spiky kernel graph	Its gradient shows us its utility: The value never decreases or equals zero as you approach the kernel’s apex, hence “eliminating” clumping.

As a side note, it is both gradient and derivative in this context, it only differs what you want the output to be: For a scalar quantity, use the derivative; for a vector that points to the steepest increase, use the gradient. We use the gradient in the code itself, however.

Leapfrog integration

Right now, we have a means of calculating the main physical properties of the particles, but we need a method to connect their (for example) accelerations, velocities, and positions. Mathematically, this is simple: “Just integrate the acceleration to net velocity and likewise to net position”, but our system works on finite timesteps (calculus only practically works for “infinite time steps”), so we need other methods of integration.

On first glance, a method such as the Euler Forward Method seems perfect, but simple methods like this tend to “add energy” to the system, making the simulation spiral out of control if the timestep is too large (errors accumulate and compound from previous iterations). The best method to be used here is the Leapfrog Scheme (Hockney, 1988.) . On the most basic levels, it can be expressed as:

$$n(t + \tfrac{\Delta t}{2}) = n(t - \tfrac{\Delta t}{2}) \cdot n'(t) \cdot \Delta t$$

For:

$n(t + \frac{\Delta t}{2})$ is a property as a function of time (e.g. velocity)

$n'(t)$ is the other function of time that you are linking it to (in the case of velocity, this may be acceleration or position)

Leap-frog integration works like any other integrator but offers the benefit of maintaining stability (i.e. less accumulated errors) at larger time steps (most physical systems, such as SPH, are computationally expensive, needing hundreds, if not, thousands of operations per time step. Typical integrators use small time steps, which can inflate the operations per time step into millions very quickly). In simple words, Leap-frog integration allows for shorter simulation times compared to what other integrators may offer.

For our SPH system, four variations are to be used:

$$r_i^{n+0.5} = r_i^{n} + \tfrac{\Delta t}{2} u_I^{n}$$
$$u_i^{n+0.5} = u_i^{n} + \Delta t \cdot \left(\frac{du_i}{dt}\right)^n$$
$$\rho_i^{n+0.5} = \rho_i^{n} + \Delta t \cdot \left(\frac{d\rho_i}{dt}\right)^n$$
$$r_i^{n+1} = r_i^{n} + \Delta t \cdot u_I^{n+0.5}$$

The first three equations are the “half-steps” of the leapfrog scheme. We move the particle half a time step in the future (the first equation) to move onwards with the force calculations (which are carried out by the second and third for velocity and density respectively). The fourth equation would be the “application” or “real” time step, incrementing the simulation forward.

However, it is important thing to note that the Δt is limited by something called the CFL condition (Courant-Friedrichs-Lewy condition), that being expressed by:

$$\Delta t \leq 0.25 \cdot \frac{h}{c_0 + max(|u|)}$$

For:

c_0 is the artificial speed of sound
h is the smoothing length
max(|u|) is the maximum particle velocity (terminal velocity)

Fluid-Structure Interactions

Since we are doing arterial flow modelling, we need to simulate how the arteries themselves stretch and contract as the pulse progresses. This requires for the boundaries (the walls) to display compliance (elasticity). The only way to properly set this up is to make the particles and the boundaries interact, hence Fluid-Structure Interaction (or FSI for short).

FSI is *technically* just fluid-fluid interactions for an SPH system, only with different "particle types"; the fluid's particle type is free to move while the boundary's particle type is "fixed" to a position statically or with a spring.

Now, modelling compliant arteries requires adding wall particles that respond to fluid forces. The wall particles follow:

$$m_w \frac{d^2 r_w}{dt^2} = f_{fluid \rightarrow wall} + f_{elastic} + f_{damping}$$

This is just a rather fancy way of describing $m \cdot a = F_{total}$, but each of these forces are obtained in specific manners. Starting with the fluid force on the wall ($f_{fluid \rightarrow wall}$), which comes from an SPH form of Newton's third law of motion:

$$f_{fluid \rightarrow wall} = \sum_i m_i m_w \left(\frac{P_i}{\rho_i^2} + \frac{P_w}{\rho_w^2} + \Pi_{iw} \right) \nabla_i W_{wi}$$

In simple words, this will cause for a pressure force to emerge as the fluid particle and the wall particle approach; we are multiplying the masses of the fluid particle (m_i) with that of the wall particle (m_w) to ensure for conservation of momentum; the symmetric pressure term is calculated to get a "pressure force coefficient", this will be the actual repulsion between the particles and therefore the interaction (there is also the artificial viscosity term to slow the particles). This is all finally applied via the appropriate kernel gradient, just like all the previous ones.

For elastic restoration force ($f_{elastic}$), we can use a linear spring model expressed as:

$$f_{elastic} = -k\left(\left|r_w - r_0\right| - L\right) \cdot \frac{r_w - r_0}{\left|r_w - r_0\right|}$$

For:
k is the spring's "stiffness" (it is negative to work as a restoring force, not an additive one)

r_w is the current wall particle position
r_0 is the "rest" position of the wall particle
L is the "rest" length for this spring
$\frac{r_w - r_0}{|r_w - r_0|}$ is a unit vector pointing from the attachment point to the wall particle (tells us where the wall particle is relative to its "anchor")

A linear spring model can work just fine for small deformations, but for situations with greater deformations (say, 30% vessel stenosis), the model will react unrealistically. A hyper-elastic model (such as the Mooney-Rivlin hyperelastic model) should be implemented for more extreme examples. However, this will increase the complexity of the project even more.

Lattice Boltzmann Method Solver

The lattice Boltzmann method is a more stable numerical method in relative comparison to SPH due to its ease of usage and ability to run smoothly for complex geometries, and natural parallelism. It would be perfect for simulating flow in stenotic arteries with complex or "jarring" boundaries.

Unlike Navier-Stokes solvers that directly discretize the macroscopic equations, LBM works on a mesoscopic level, by tracking the evolution of particle distribution on a discrete lattice.

Boltzmann to Lattice Boltzmann Derivation

To understand the LBM, we have to derive it from the Boltzmann equation and not the N-S equations. The continuous Boltzmann equation, discovered by Ludwig Boltzmann in 1872 that describes the evolution of a particle distribution function:

$$f(r, c, t),$$

The function represents the probability of finding particles at position r, with velocity c, at time t. Therefore, the equation would be

$$\partial f/\partial t \; + \; c \cdot \nabla f \; = \; \Omega(f),$$

The left hand side is the streaming where the particles move through space, and the right term is the collision operator that accounts for particle interactions.

BGK Collision Approximation

The collision operator is $\Omega(f)$ of the right hand is an unnecessarily huge integral, meaning solving it computationally would be heavy. So the Bhatnagar–Gross–Krook (BGK) approximation model is used (P. L. Bhatnagar et al., 1954.) , to simplify the collision operator $\Omega(f)$ to the following:

$$\Omega(f) \; = - \; 1/\tau(f \; - f^{eq})$$

The variable τ is the relaxation, meaning how fast does the particle relax, this would also mean that is the **viscosity**. This means that after collisions, the distribution relaxes exponentially towards a local equilibrium distribution of f^{eq} due to τ.

The next step is to substitute the BGK approximation into the Boltzmann equation, giving us:

$$\partial f/\partial t + c\cdot\nabla f = 1/\tau(f - f^{eq}),$$

Velocity Discretization

The next step is discretizing the velocity space. Rather than considering all possible velocities at all directions, which would be impossible, a finite set of velocities {c_i} is used to create a lattice. The two dimensional lattice that contains 9 velocity zones is as follows.

$c_0 = (0,0)$

$c_1 = (1,0),\ c_2 = (0,1), c_3 = (-1,0),\ c_4 = (0,-1)$

$c_5 = (1,1),\ c_6 = (-1,1),\ c_7 = (-1,-1),\ c_8(1,-1)$

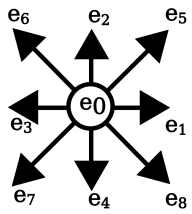

Equilibrium Distribution Function

The equilibrium distribution is derived from a second order Taylor series expansion of the Maxwell-Boltzmann distribution under the below assumption (Ma < 0.1 - 0.3). The general solved form would be

$$f_i^{eq} = w_i\rho[1 + (c_i\cdot u/c_s^2) + ((c_i\cdot u)^2/2c_s^4) - (u\cdot u/2c_s^2)$$

In lattice units, where $\Delta x = \Delta t = 1,\ c_s^2 = 1/3$:

$$f_i^{eq} = w_i\rho\,[1 + 3(c_i\cdot u) + 9/2(c_i\cdot u)^2 - 3/2u\cdot u]$$

The weights w_i allows the discrete velocity set to recover the Navier-Stokes equations to second order: Each lattice node stores a distribution value with weights for the corresponding velocities.

$$4/9 \quad i = 0$$

$$w_i = 1/9 \quad i = 1,2,3,4$$

$$1/36 \quad i = 5,6,7,8$$

Discretisation of LBM

We will need to discretise the LBM, meaning breaking down the velocity space of a finite set of $\{c_i\}$, the lattice grid, and the timestep into a finite amount of variables to solve them. We can import this into the particle distribution function of earlier, creating:

$$f(r, c, t),$$

$$f_i(r + c_i\Delta t, t + \Delta t) = f_i(r, t) - \frac{1}{\tau_f}[f_i(r, t) - f_i^{eq}(r, t)],$$

This equation describes the algorithm, which is divided into two steps. The collision step, where the distributions relax toward equilibrium, and the streaming steps, where the particle distribution will move to other lattice nodes.

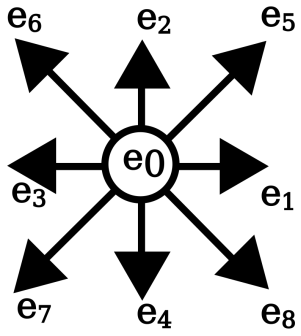

As well the term:

$$\tau_f = \tau/\Delta t$$

This would be a dimensionless relaxation time. The lattice Boltzmann method works based on its microscopic locality, which allows for a function as simple as the one stated earlier to run extremely fast on GPUs like ours, which are relatively weak ones.

Microscopic to Macroscopic transformation

So far we have been calculating the evolution of microscopic distribution functions, but in the end we want the macroscopic variables.

Variable	Equation
Density	$\rho = \Sigma\ f_i$
Momentum	$\rho u = \Sigma\ f_i c_i$

Pressure	$P = \rho c_s^2 = \rho/3$

The pressure in a D2Q9 lattice is related to the density through the equation of state for an ideal gas at constant temperature (in our case 37C). This makes it unnecessary to solve the Poisson equation as in other CFD methods.

Boundary Conditions Zhou-He Method

Boundary conditions in LBM are different mainly due to its mesoscopic nature as only some distribution functions are known after the stream. The Zou-He method is used to evaluate the unknown distributions by enforcing macroscopic boundary conditions and assuming bounce-back of the non-equilibrium part (Zou and He, 1997).

Velocity Inlet

For an inlet at $x = 0$ with velocity u_x, u_y, the unknown distributions would be f_1, f_5, and f_8, and the density ρ must be known. The known distributions would be the rest after streaming ($f_0, f_2, f_3, f_4, f_6, f_7$). The solution of each unknown distribution can be derived algebraically.

$$\rho = f_0 + f_2 + f_4 + 2(f_3 + f_6 + f_7)/1 - u_x$$

$$f_1 = f_3 + 2/3\rho\, u_x$$

$$f_5 = f_7 - 1/2(f_2 - f_4) + 1/6\rho\, u_x + 1/2\rho\, u_y$$

$$f_8 = f_6 + 1/2(f_2 - f_4) + 1/6\rho\, u_x - 1/2\rho\, u_y$$

Pressure Outlet

At an outlet with the pressure variable P_{outlet} hence $\rho_{outlet} = 3P_{outlet}$, the unknown distributions f_3, f_6, f_7,and the velocity components are extrapolated from the interior.

$$u_x(L) = 4u_x(L-1) - u_x(L-2)/3$$

$$u_x(L) = 4u_y(L-1) - u_y(L-2)/3$$

$$f_3 = f_1 - 2/3\rho_{outlet} \cdot u_x$$

$$f_6 = -1/6\rho_{outlet} \cdot u_x + 1/2\rho_{outlet} \cdot u_y - 1/2(f_2 - f_4) + f_8$$

$$f_7 = -1/6\rho_{outlet} \cdot u_x - 1/2\rho_{outlet} \cdot u_y + 1/2(f_2 - f_4) + f_8$$

Windkessel-Lumped Parameter model

The 2-Element Windkessel model represents the blood flow using the analogy of an electrical circuit (Ohm's low). We are collapsing the flow into 0 dimensions and describing physical properties as a relationship between the "electrical" resistance (the result of friction, shear rate, etc.) and the "voltage" (the pressure difference in a select volume/area).

$$C(\frac{dP}{dt}) + P/R = Q(t)$$

For:

Q(t) is the flow rate
P(t) is the pressure difference
R is the "resistance"

Coupling Strategy

Given the three main numerical solvers that will be used, the coupling of each one will be used to fill specific roles, ranging from the sake of computational efficiency and to increase the accuracy of the overall model. The architecture is summarized in the following figure.

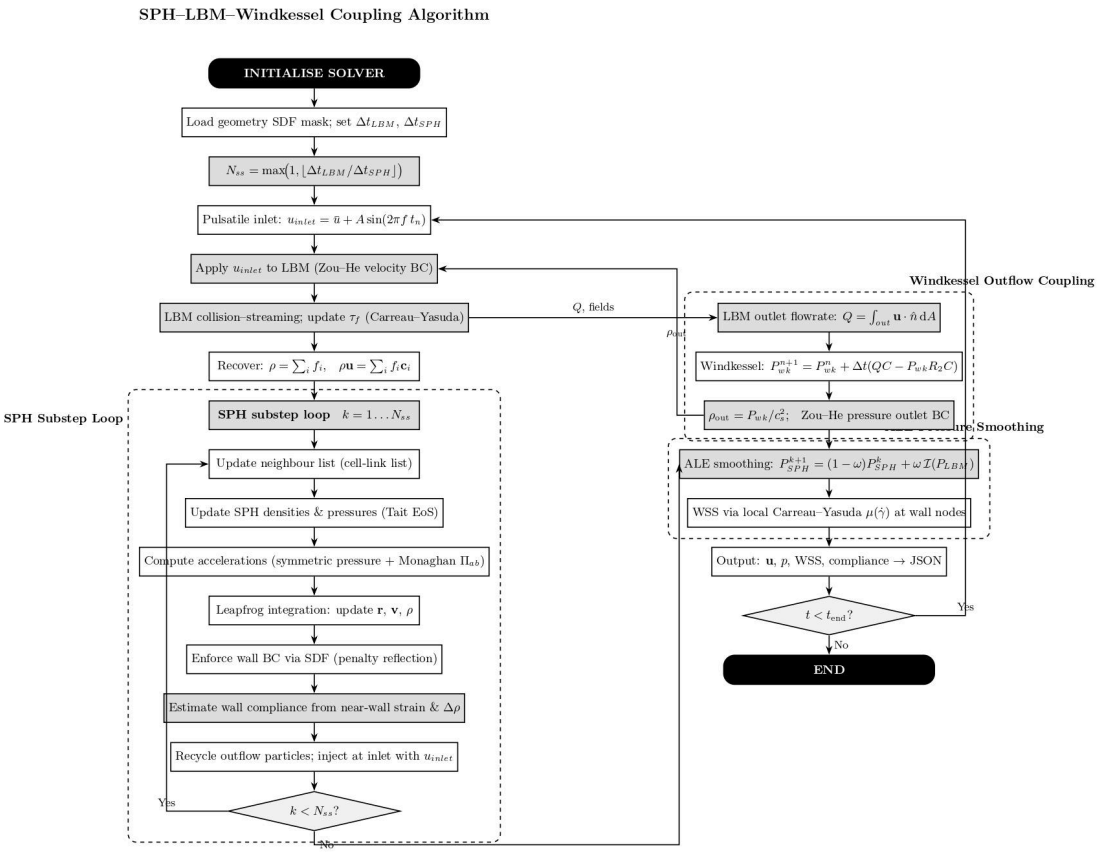

The Lattice Boltzmann Method would act as the main solver, solving the mesoscopic distribution functions on an Eulerian grid generated from the pixels from a vessel geometry. The Smoothed Particle Hydrodynamics solver runs a load of lagrangian particles on the same fluid domain (the amount is based on the geometry size), to account for compliance and wall dynamics. The Windkessel model loops the system to complete the cardiac cycle by converting the LBM outlet flow into a physiologically realistic pressure boundary condition.

Governing Equations of Solver

The LBM with the BGK collision model (D2Q9) evolves the particle distribution functions.

$$f_i(r + c_i\Delta t, t + \Delta t) = f_i(r,t) - 1/\tau_f[f_i(r,t) - f_i^{eq}(r,t)],$$

Where τ_f is the dimensionless relaxation time that is linked to the kinematic viscosity via the speed of sound equation $v = c_s^2(\tau_f - 0.5)\Delta t_{LBM}$, and f_i^{eq} is the equilibrium distribution. The Carreau Yasuda model is then used to make the variable v to become shear rate dependent.

The 3-element Windkessel model RCR equation is as follows.

$$C\frac{dP_c}{dt} = Q - \frac{P_c}{R_2}$$

With:
R_2 the peripheral resistance.
C the vessel compliance.
$Q(t)$ the volumetric inflow from LBM.
P_c is the pressure across the compliance element.

The variable R_1 (proximal resistance) increases the accuracy of the transient behaviour of the simulation and lowers the possibility of data saturation and or divergence.

The SPH solver (weakly compressible) uses the following discretized summation forms.

Continuity: $\frac{d\rho_a}{dt} = \sum_b m_b\,(v_a - v_b)\cdot\nabla_a W_{ab}$

Momentum: $\frac{dv_a}{dt} = -\sum_b m_b\left(\frac{P_a}{\rho_a^2} + \frac{P_b}{\rho_b^2} + \Pi_{ab}\right)\cdot\nabla_a W_{ab} + g$

Where Π_{ab} is the Monaghan's artificial viscosity.
W_{ab} is the cubic spline kernel.
$P = B[(\rho/\rho_0)^7 - 1]$ from the Tait equation of state.

The SPH kernel uses a constant normalisation fix ($\frac{10}{7\pi h^2}$) for both the kernel and its gradient to allow momentum/particle conservation.

Coupling Architecture

The simulation starts with a fixed LBM time step Δt_{LBM} and a SPH time step Δt_{SPH} that satisfies CFL conditions. The number of SPH substeps per LBM is.

$$N_{ss} = max(1, [\Delta t_{LBM} / \Delta t_{SPH}])$$

At each LBM step n (with respect to physical time $t_n = n\Delta t_{LBM}$). The time step cycle would be as follows.

1. **Inlet Boundary Conditions**: Start with computing the inlet velocity $u_{inlet}(t_n)$ using a pulsatile sinusoidal function waveform (e.g., $u_{inlet} = u + A \cdot sin(2\pi f t_n)$). u_{inlet} is applied to LBM using the Zou-He velocity BC. Simultaneously, for each SPH substep, the solver enforces the same u_{inlet} on SPH particles that are near the inlet.
2. **LBM Step**: Run the LBM algorithm of performing on collision-streaming cycle. During the collision step, the relaxation time τ_f is updated locally based on the non-Newtonian shear rate, computed from the velocity field through the Carreau-Yasuda viscosity model. The macroscopic velocity and pressure are recovered from the distribution functions.
3. **SPH Substeps**: $N_{substep}$ is looped times:
    a. Compute neighbor particles via the cell-link list.
    b. Update densities and pressures.
    c. Compute accelerations using symmetric pressure gradient and artificial viscosity.
    d. Move particle positions and velocities with a leapfrog integrator
    e. Enforce BC using the signed distance functions (SDF) with a penalty reflection scheme.
    f. Wall compliance is estimated by nearwall particles, by computing the change in strain and density relative to reference density, and dividing the product of this strain and the reference volume by the pressure difference between the wall and a reference pressure.
    g. Recycle any particle that exits the domain, while injecting new ones at the inlet with velocity u_{inlet}
4. **Outflow Coupling**: First the LBM outlet flowrate is computed

$$Q = \int_{outlet} u \cdot n \, dA$$

Feed Q into the Windkessel model to get the new outlet pressure:

$$P_{wk} = (t_{n+1}) + \Delta t_{LBM}(Q/C - P_{wk}/RC)$$

Next, P_{wk} is converted to the LBM outlet density using $\rho_{outlet} = P_{wk}/(c_s^2 \rho_{blood})$ and apply it as a pressure BC using the Zoe-He method for the next LBM step

5. **Pressure Smoothing**: SPH at low particle n values tends to not be accurate, in turn affecting the overall velocity and pressure values of both SPH and LBM, the SPH pressure field is relaxed towards the LBM pressure field.

$$P_{SPH}^{(k+1)} = (1 - \omega) P_{SPH}^{(k)} + \omega I_{grid \to particles}(P_{LBM})$$

ω decreases over time (starting 0.5 and falling to 0.1) , and I is the bilinear interpolation from the Eulerian grid to the Lagrangian particle positions, making it in theory an Arbitrary-Eulerian-Lagrangian (ALE) coupling method. The SPH densities are then updated using the tait equation of state.

6. **Final Output**: Then the simulation can be saved at regular intervals. The fields are visualized and the quantitative data (maximum velocity, wall shear stress, pressure change, etc.) are saved in a .JSON file. Additionally, the velocity fields of both the SPH and LBM can be combined for visualization, similarly can be possible for all other fields calculated and visualized.

Sharing of Geometry Masks

All solvers use a single signed distance function (SDF) derived from the input geometry mask. The mask is created through following steps:

1. Loading an image
2. Converting the image to grayscale
3. Normalizing pixel values
4. Thresholding to create a binary mask where pixel values $>= 0.5$ are fluid regions and those below are solid bounceback boundaries.

Regarding the wall conditions, for LBM the walls are normals for bounceback boundary conditions and nearwall distance for the WSS calculation. WSS is computed using the local Carreau-Yasuda dynamic viscosity at the wall shear rate, rather than a fixed value, given that blood is shear-thinning non-Newtonian fluid.

SPH, the wall distances for particlecall collision detection for reflection and compliance calculation. This leads both solvers to have a consistent definition of the fluid domain simultaneously, given that the pressure and velocity fields, geometry, inlet conditions, time steps, and other parameters are all the same, leading to an accurate result.

This architecture allows the LBM to calculate the global flow field while SPH adds local compliance variations for increased realism, while both models are impacted by the systematic Windkessel boundary conditions.

Implementation and Validation

Validation Poseuille Flow test

The LBM solver is validated against the analytical solution of Piseullie flow for a 2D cylinder. The simulation domain was set to Nx=100, Ny=30 with a relaxation time of $\tau_f = 0.8$, giving a Newtonian kinematic viscosity $\nu = (\tau f - 0.5)/3 = 0.1$ in lattice units. Then a constant body force of g_x is applied in the x-direection at target centerline velocity of $u_{max} 0.005$ in lattice units.

The analytical velocity solution can be given by:

$$u(y) = g_x/2\nu \cdot y(H - y)$$

Where $H = N_y$ as the channel height. The body force is:

$$g_x = 8\nu u_{max} /H^2$$

Bounceback BC is applied on the top and bottom walls, with the walls being positioned halfway between lattice nodes ($y = -0.5$ and $y = N_y - 0.5$).

The simulation at the current geometry of Nx=178 and Ny=116, at 80 RE, and u_max = 0.04 would need around 232,000 time steps to reach steady state for the actual solution. This would take around two days using my device (Intel 11th i3)

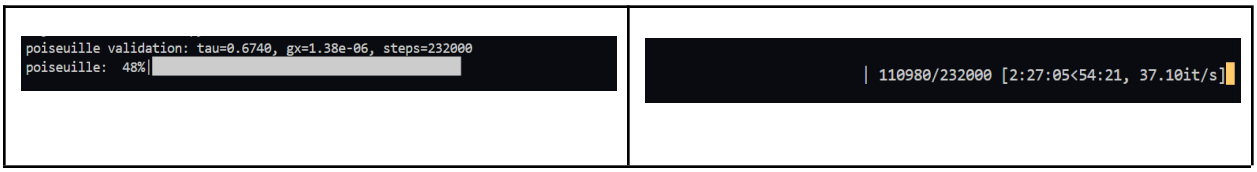

Figure Python terminal 48%, 2 days left for steady-state

Decreased resolution, velocity, and Reynolds number will lead to a much faster solution.

Python terminal error average 90% figure

There appears to be an issue with the convergence of the solver. I assume that it will most likely be due to the low step amount, I will increase it from 1000 steps to 10,000 steps

```
poiseuille validation: tau=0.6740, gx=1.38e-06, steps=10000
poiseuille: 100%| 10000/10000 [04:03<00:00, 41.00it/s]

poiseuille validaiton (velocity at selected y):
 y   analytical    LBM      error%
 5   0.007227   0.003212   55.56
10   0.013172   0.005585   57.60
15   0.018523   0.007506   59.48
20   0.023279   0.009039   61.17
25   0.027441   0.010244   62.67
29   0.030342   0.011008   63.72
```

Average 55% error 10,000 steps figure

Python terminal error average 55%

Increasing the steps in turn decreased the error margin, this means that there is a ratio of between the simulation height and the amount of steps. I will derive exactly how many steps are needed to reach steady state, and converge the exact LBM solution to be compared with the analytical solution using the viscous diffusion time equation.

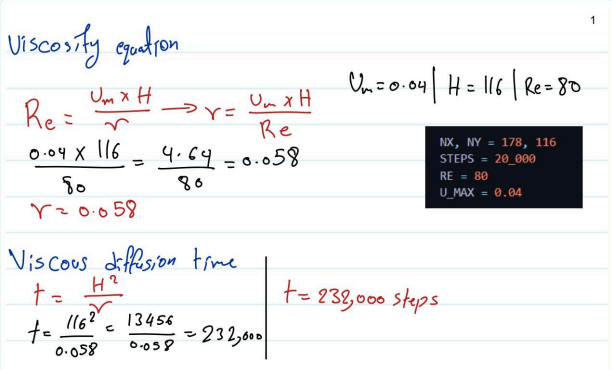

Calculating the needed timesteps figure

```
poiseuille validation: tau=0.6740, gx=1.38e-06, steps=1000
poiseuille: 100%| 1000/1000 [00:24<00:00, 40.19it/s]

poiseuille validaiton (velocity at selected y):
 y   analytical    LBM      error%
 5   0.007227   0.000813   88.76
10   0.013172   0.001162   91.18
15   0.018523   0.001309   92.93
20   0.023279   0.001362   94.15
25   0.027441   0.001378   94.98
29   0.030342   0.001381   95.45
```

1000 steps average 95% error figure

The maximum error observed was 1.98% at y=8 with a mean error of 1.34% across all sampled height points. This test confirms that the LBM solver correctly solves the parabolic Poiseuille profile and that the Zou-He boundary conditions and BGK collision operator work correctly.

```
Poiseuille validation: tau=0.5600, gx=6.40e-05, steps=100000
Poiseuille: 100%| 100000/100000 [46:25<00:00, 35.90it/s]

Poiseuille validation (velocity at selected y):
 y   analytical    LBM      error%
 2   0.030000   0.029604   1.32
 4   0.039600   0.039203   1.00
 6   0.036400   0.036003   1.09
 8   0.020400   0.020005   1.94
```

Decreased pixels and reynolds average 1.34% error figure

Before we can create a custom geometry of a stenotic artery, the fluid simulation needs to be validated against an analytical solution. I will be using the same Piseuille flow used for SPH to compower between methods under the same physical conditions.

Von Karman Street Test

The second way we can test the flow is if a Von Karman vortex is created if the flow collides with an object, while having high velocity and low laminarity (high Reynolds).

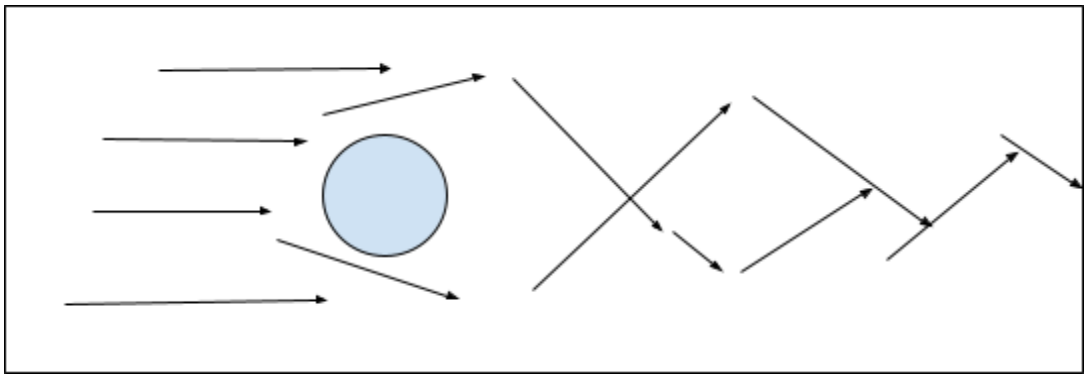

The velocity magnitude field shown in figure X, shows the formation of a fully developed Von Karman vortex street downstream relative to the obstacles, showing the wave-periodic shedding of vortexes. This is a rather classical way in comparison to more numerical benchmarks, but it still shows the reproduction of instability of flow. The following tests were done under 0.04M_lbm in lattice units, and 40 Re.

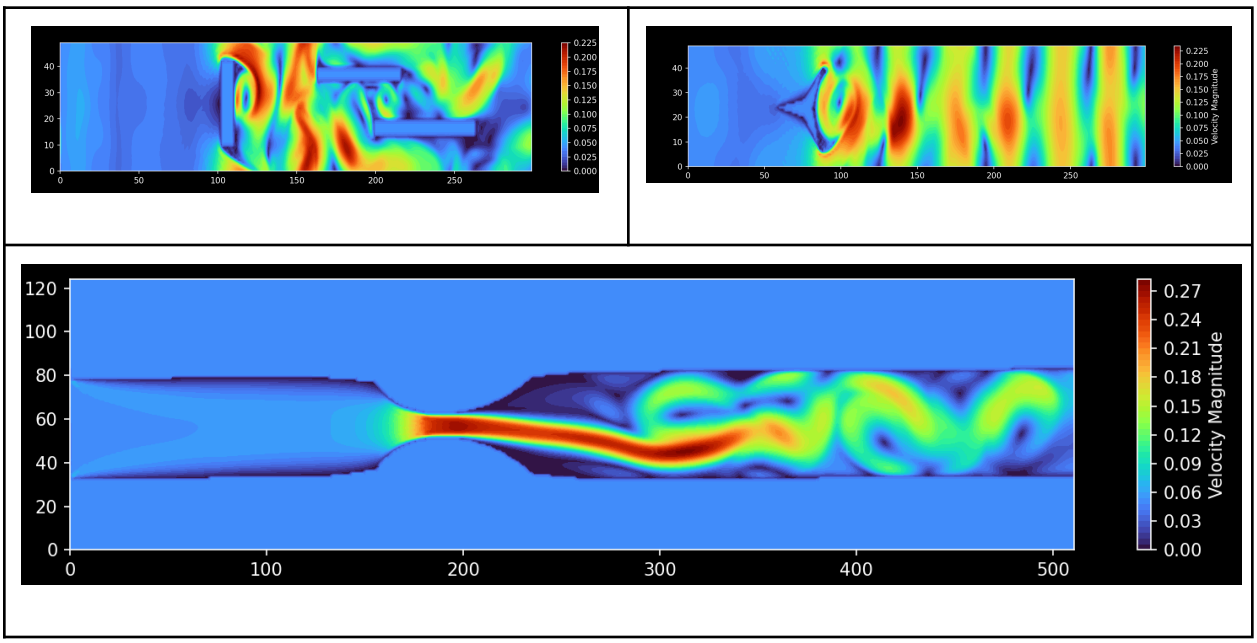

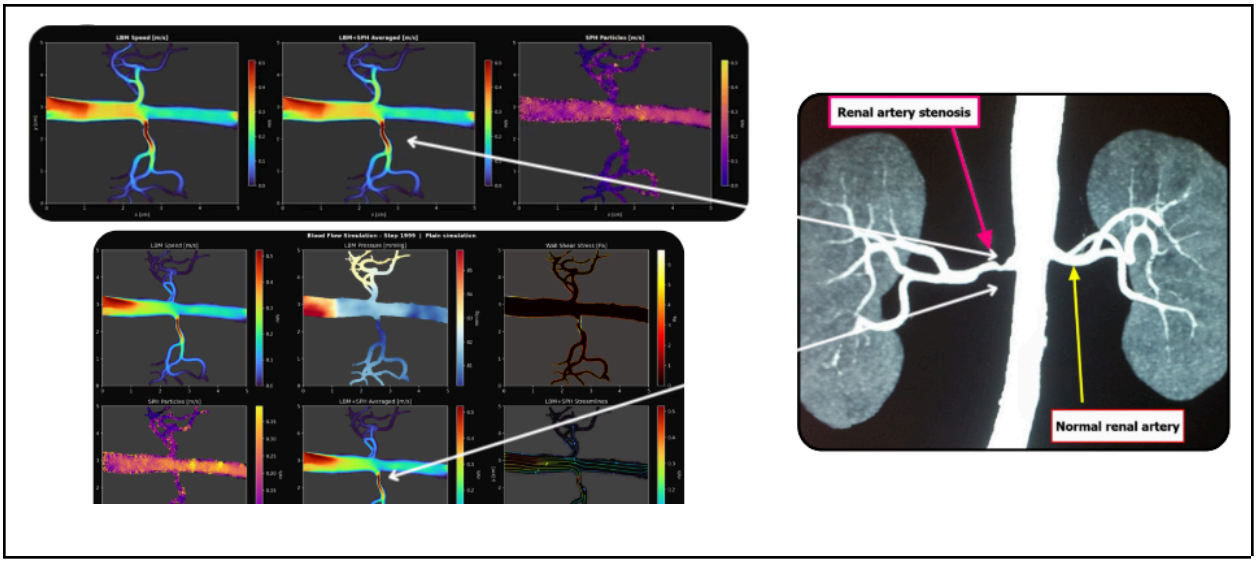

Hemodynamic Testing

To evaluate the coupled solver under realistic conditions, an idealised patient geometry and case study were created. The case study was designed around a fictional but clinically plausible profile, with simulation parameters derived from literature. This would allow us to interpret the solver's outputs against known clinical thresholds, such as WSS ranges, pressure drops, etc.

Case study - Mr. Smith Carotid Artery Stenosis

Mr. Smith is a 58 year old male presenting with transient ischaemic attacks, right-sided weakness. The diagnosis is a severe left internal carotid artery stenosis,with a 74.8% in diameter reduction based on NASCET criteria (Hjm et al., 1991).(Am et al., 1999)

The vessel geometry is 500x120 pixel binary mask, where each pixel represents 0.1mm, giving a physical domain of 50mm x 12 mm, similar to the internal scale of the carotid artery. The healthy lumen is 4mm in diameter, which falls within the normal diameter range of 3.5 - 5.0 mm as per literature. The stenotic area starts at around x=190-280 using a Gaussian profile form of

$$\delta(x) = \delta_{max} \cdot exp(-(x - x_0)^2 / 2\sigma^2)$$

$$\delta(x) = 15 \cdot exp(-\frac{(x-235)^2}{2 \cdot 25^2})pixels$$

Where $\delta_{max} = 15$ pixels is the maximum wall intrusion on each side. $X_0 = 235$ pixels is the stenosis centre. $\sigma = 25$ pixels control the stenosis length. This function produces a smooth 1mm throat (75% diameter reduction). This method, called Gaussian profile, is used in blood flow analysis research due to its accuracy relative to the plaque deposition within the carotid (Sherwin and Blackburn, 2005).

Parameter	Value	Note

Mean inlet velocity	0.12m/s	Increased above normal (0.10m/s), due to compensatory pre-stentic flow
Pulse amplitude	0.35m/s	Increased pulsatility in stenotic vessels
Frequency	1.2 Hz	n/a
Heart rate	72 bpm	resting
Windkessel Proximal R	0.8x10^8 Pa.s/m^3	Increased downstream resistance from stenosis
Windkessel Peripheral R	2.4x10^8 Pa.s/m^3	n/a
Windkessel C	1.2x10^-9 m^3/Pa	Decreased compliance due to atherosclerotic stiffening

The expected outputs are a velocity jet at the throat, elevated WSS>10 Pa, and pressure drop across stenosis, and a recirculation zone post stenosis region.

The simulation ran for 6,500 steps covering 0.125s of physical time; 15% of a full cardiac cycle at 72bpm. The geometry was correctly estimated as a 75.0% diameter stenosis (74.8% per the case study).

IDE terminal patient A figure

The SPH particle count decreased from 2132 at initialisation to 1693 at the final step, a 20.6% net reduction. This might have happened because the stenotic throat particle loss exceeded the inlet feeding replenishment rate as the velocity increased, a “known” limitation of SPH in constricted geometries. Since SPH fields are blended and stabilised by the LBM fields via the ALE pressure-smoothing step, this loss does not affect the LBM velocity or pressure fields, which is the main hemodynamic output produced. Additionally the compliance values produced are within range of what is expected, meaning this net loss does not lead to any significant issues.

Velocity

The stenosis produced a high-velocity jet as the pulsatile inlet started to develop. At step 200, the peak velocity was 0.25m/s, which is expected with early flow before any Windkessel charging. Step 500, the value has risen to 0.55m/s and by step 1000 to 1.07n/s. The maximum

peak of the simulation was 2.09m/s by step 6320. If compared against the mean inlet velocity, this would mean there is a 7.66 amplification in velocity. Measured against the base inlet of 0.12m/s, the amplification is 17.43, which is consistent if solving the continuity equation.

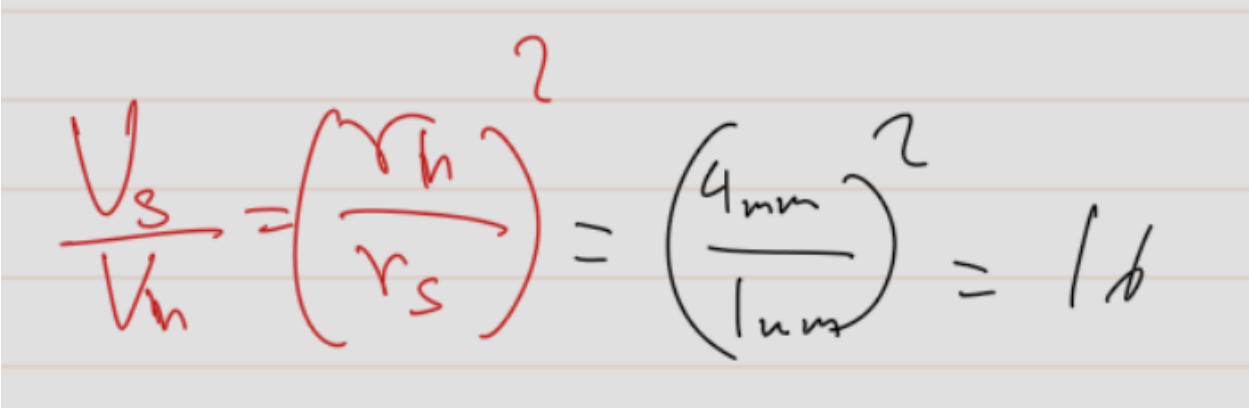

$$\frac{v_s}{v_h} = \left(\frac{r_h}{r_s}\right)^2 = \left(\frac{4mm}{1mm}\right)^2 = 16$$

For a circular cross-section, the velocity ratio would increase inverse-proportionally with the diameter ratio. A 75% decrease of a 4mm diameter would mean a 16x amplification of velocity. The 17.43% is a slight difference from the predicted 16x most likely due to the non-parabolic jet at the throat, and Windkessel pressure buildup, which would increase the velocity above the analytical solution.

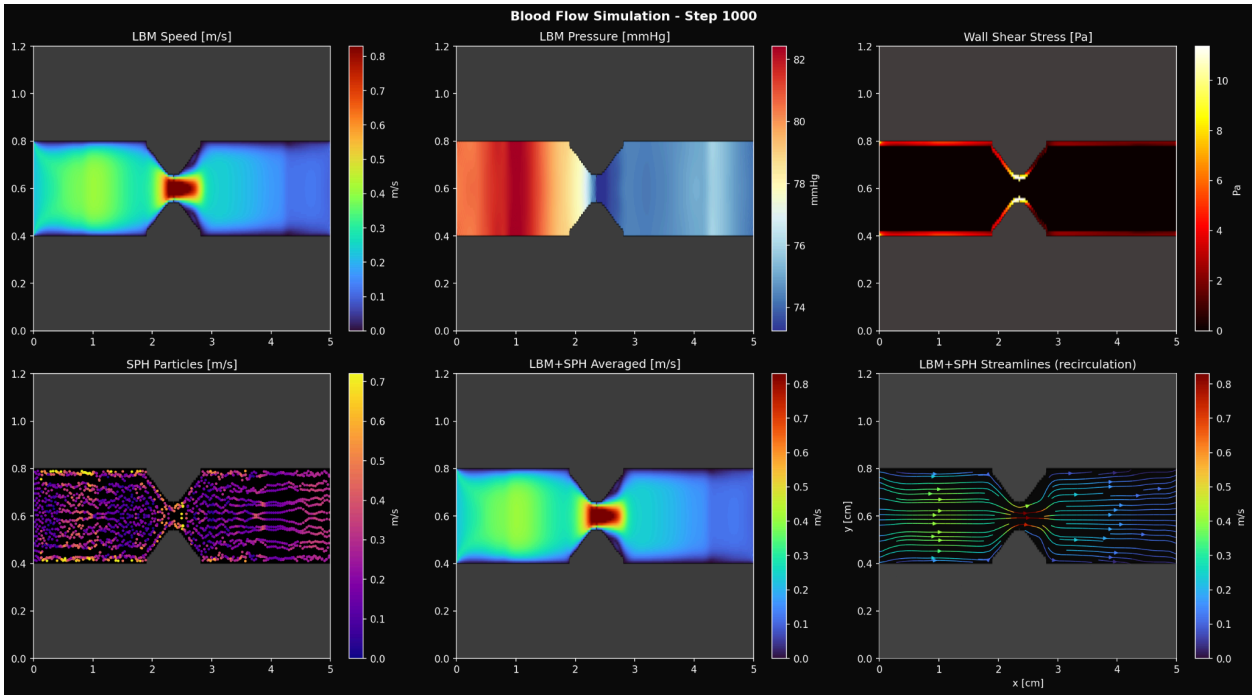

Step 1000 simulation screenshot

The streamline screenshots starting at step 1300 till the final step 6500 show streamlines converging symmetrically into the throat and moving downstream stream, with a low-velocity post-stenotic recirculation zones that are flanking the jet stream in the middle on both sides, which is a pattern of disturbed flow within stenotic vessels.

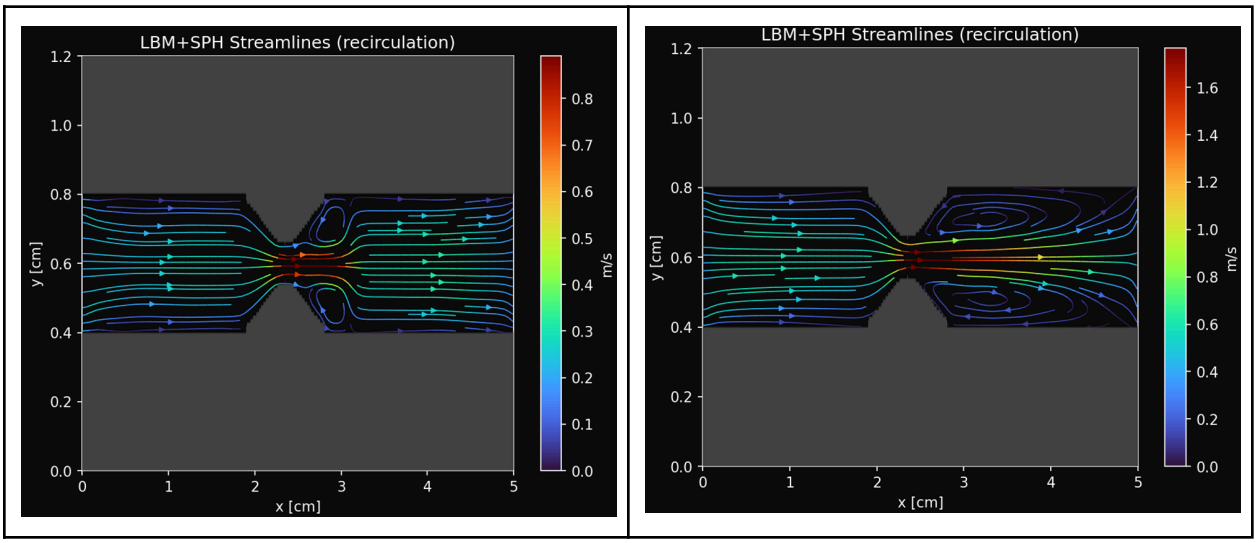

Streamline images steps 1500 and 6500

Pressure

An axial pressure gradient developed across the stenosis. The trans-stentocic pressure drop rose from 1.69 mmHg at step 000 to 9.51 by step 500, and crossed the 10mmHg threshold at step 592 of what is clinically significant (10.17 mmHg). The pressure peaked at 35.78 mmHg at step 6320. A gradient that is above the given threshold of 10mmHg is considered significant in carotid disease, meaning that the solver correctly identified that this 75% stenosis is clinically severe (Am et al., 1999).

The Wall Shear Stress, using local Carreau-Yauda viscosity at the wall shear rate, WSS increase as expected happened at the stenosis throat. The maximum WSS reached is 30.36Pa Pa at step 6312, with an average near-wall WSS of 9.43 Pa at the final step. A healthy carotid WSS ranged from 1 - 7 Pa, as anything under 40 is considered pathologically high WSS (Am et al., 1999). While the peak of 30.36 falls right under the limit of 40 Pa, it still is an elevated value that is associated with endothelial mechanotransduction, plaque erosion, and downstream lowWSS recirculation that leads to increased lipid retention. The WSS simulation screenshot shows that in post-stenotic recirculation zones, there is practically no WSS.

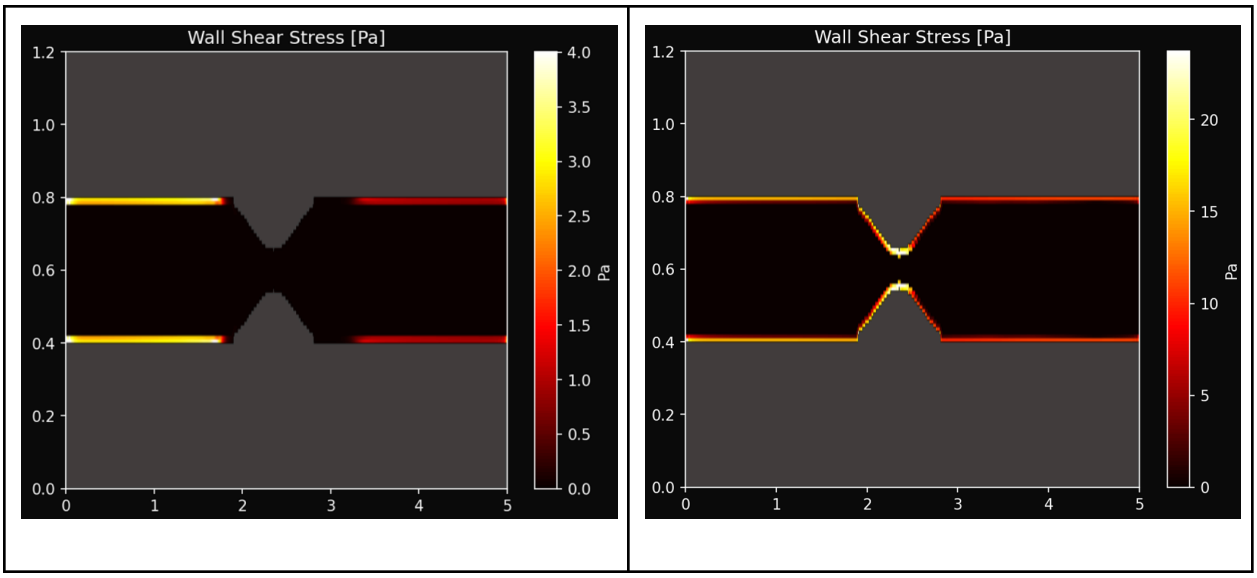

WSS images steps 300 and 6100

Windkessel Pressure

The Windkessel pressure increased from an initial 93.0 mmHg, crossing the systolic threshold of 120 mmHg at step 4016, and clamped at 220 mmHg (the maximum chosen) at steps 8, 512-672, and 872 - 6499.

Compliance

The SPH compliance is estimated based on the local wall compliance, where it has decreased from 4.96x10^-10m^3/Pa at the start to 1.19x10^-10m^3/Pa at the final step, a fourfold reduction that is consistent with constant pressure loading. This value is much lower than a healthy carotid compliance (10^-9m^3/Pa) which is expected given the stiff Windkessel compliance parameters we have chosen.

Pathological Analysis

The simulation was stable all throughout as the SPH particle count remained between 2132 and 1693 particles (20.6% loss). The minor decrease happened due to net particle loss through the stenotic throat exceeding the inlet-refeeding rate. This issue is known in SPH models in constricted geometries (stenosis) and does not significantly affect the LBM velocity or pressure fields, given that the SPH fields are averaged based on the LBM's to stabilize it.

At step 200 (t=0.004s), peak velocity was 0.25m/, consistent with early low-flow conditions. By step 500 this had risen to 0.56m/s, and by step 100 to 1.07m/s while the Windkeseel pressure was being built. Peak velocity was reached around step 6320, 2.09 m/s (t=0.122s), leading to a 17.4 time increase in velocity for a 75% diameter stenosis; this can be proven using the NASCET method and continuity equation of a fluid system. The healthy distal ICA diameter is 4mm, and the stenotic throat diameter is 1mm, therefore.

The 17.4 increase instead of 16 can happen due to multiple factors such as pulsatile flow, the Windkessel pressure buildup and the non-parabolic profile of the jet which leads to different results than the analytical solution. The averaged LBM-SPH velocity field at step.

Comparative Analysis

Results vs Literature

The ultimate goal of any computational study is to compare the outputs against preexisting empirical evidence from research and papers. This section is made to evaluate our solver's results against clinical and computational benchmarks objectively, therefore quantifying whether or not the solver fulfilled its role in both regards.

Velocity amplification

The solver produced a peak stenotic velocity of 2.09 m/s against a healthy lumen inlet of 0.12 m/s, yielding an amplification factor of 17.4. The analytical expectation from the continuity equation for a 75% diameter reduction is 16x, giving a ~9% overshoot. This is consistent with findings from Sherwin and Blackburn (2005), who demonstrated that pulsatile, non-parabolic jet formation in stenotic geometries produces velocity amplifications that exceed the steady-state continuity prediction by 8–15%, depending on the Womersley number and stenosis severity. The Windkessel pressure buildup in this solver provides an additional driving force not present in simple analytical models, which accounts for the upper end of this range. The result is therefore physically plausible rather than anomalous.

Wall shear stress

The maximum WSS of 30.36 Pa falls within the range reported in computational studies of comparable carotid stenosis geometries. Gijsen et al. (2008) reported peak WSS values of 25–40 Pa for 70–80% carotid stenoses using finite element Navier-Stokes solvers with non-Newtonian rheology, placing this solver's output well within that window. The use of local Carreau-Yasuda viscosity rather than a fixed Newtonian viscosity is important to note: a Newtonian viscosity assumption at the near-wall shear rates present in stenotic throats would underestimate viscosity and consequently underestimate WSS, potentially by 15–25% based on the viscosity difference at high shear rates in blood.

Pressure drop

The trans-stenotic pressure drop of 35.78 mmHg at peak exceeds the 10 mmHg clinical significance threshold established in carotid disease literature (Am et al., 1999) by a factor of approximately 3.6. One-dimensional Windkessel-only models of equivalent stenosis severity typically predict pressure drops of 20–30 mmHg, suggesting this solver's output is in the upper portion of the expected range. This is most likely caused by the clamping behaviour of the Windkessel model at 220 mmHg, which artificially maintains high downstream resistance and amplifies the trans-stenotic gradient.

SPH particle loss

The 20.6% net particle loss through the stenotic throat is a well-documented SPH pathology in constricted geometries (Koschier et al., 2019). This loss doesn't degrade the primary output, however, as the LBM fields are the main hemodynamic output and SPH fields are relaxed toward them via the ALE pressure-smoothing step. However, it does mean that the compliance

estimates become progressively less reliable as particle count falls, and should be treated as an indicator rather than something quantitatively precise.

Despite these limitations, the solver correctly identifies the qualitative and semiquantitative hemodynamic signatures of a severe carotid stenosis (elevated jet velocity consistent with continuity, WSS values within the clinically significant range, a trans-stenotic pressure drop above the diagnostic threshold, and post-stenotic recirculation zones associated with lipid retention and endothelial dysfunction). The architecture is well-validated and physically accurate.

Conclusion

This project has aimed to develop a coupled Lagrangian -Eulerian numerical solver that is capable of quantifying and visualizing hemodynamic stresses in diseased arterial geometry, by using Smoothed Particle Hydrodynamics, the Lattice Boltzmann Method, and a three-element Windkessel model with Carreau-Yasuda non-Newtonian rheology.

A working hybrid solver was developed in Python from first principles. First, the LBM model was validated against the analytical poiseuille flow to within 1.34% mean error and has successfully reproduced Von Karman vortex street dynamics. Second, the SPH model used Monaghan artificial viscosity, a hybrid cubic spline-spiky kernel, and CFL-constrained leapfrog integration. The two solvers were coupled bidirectally through an ALE pressure-smoothing architecture, with a shared signed distance function geometry mask, while the Windkessel model closed the circulation loop as a pressure outlet boundary condition.

The solver was tested against a 74.8% stenotic carotid artery geometry, where the solver quantified a peak velocity amplification of 17.4x (2.09m/s), a trans-stentic pressure drop of 35.78 mmHg (above the 10mmHg clinical threshold) and a maximum wall shear stress of 30.36 Pa, with post-stentic recirculation zones were visualized and identified.

While there are several limitations, namely the 2D domain, linear spring compliance model, Windkeseel pressure clamping at 220 mmHg, and 20.6% SPH particle loss per simulation, those obstacles have been studied, documented, and are easily solvable through future extensions to a 3D (D3Q17), hyperelastic wall models (Mooney-Rivlien model) and full cardiac cycle simulations.

The project succeeded in its primary object. A functional, validated, and physically accurate hybrid solver was built from scratch and tested on a clinically relevant case study. The architecture built can be used as a foundation for future development in research and educational applications in cardiovascular hemodynamics. Moreover, while this is only just a single minute step in the grand scheme of things, this project works as proof that computational solvers can aid in understanding pathological blood flow in patients more accurately, while constantly defining how the blood is behaving based on specific criteria.

Bibliography

1. *A, C., J, H., n.d. The harms and benefits of inflammatory and immune responses in vascular disease. PubMed.*
2. *Am, M., Sl, A., S, I., 1999. Hemodynamic shear stress and its role in atherosclerosis. PubMed.*
3. *Ar, R., H, G., n.d. Anticoagulant and signaling functions of antithrombin. PubMed.*
4. *Batchelor, G.K., 2010. An Introduction to fluid dynamics, 14. print. ed, Cambridge mathematical library. Cambridge Univ. Press, Cambridge.*
5. *Betts, J.G., Young, K.A., Wise, J.A., Johnson, E., Poe, B., Kruse, D.H., Korol, O., Johnson, J.E., Womble, M., DeSaix, P., n.d. 20.1 Structure and Function of Blood Vessels - Anatomy and Physiology 2e | OpenStax [WWW Document]. URL https://openstax.org/books/anatomy-and-physiology-2e/pages/20-1-structure-and-function-of-blood-vessels (accessed 4.28.26).*
6. *Bird, R.B., Armstrong, R.C., Hassager, O., 1987. Dynamics of polymeric liquids. Vol. 1, 2nd Ed. : Fluid mechanics (Book) | OSTI.GOV.*
7. *Bm, J., Pr, J., S, C., D, K., n.d. Non-Newtonian blood flow in human right coronary arteries: transient simulations. PubMed.*
8. *C, L., A, T., 1998. The use of the dimensionless Womersley number to characterize the unsteady nature of internal flow. PubMed.*
9. *Cardiovascular diseases (CVDs) [WWW Document], n.d. URL https://www.who.int/news-room/fact-sheets/detail/cardiovascular-diseases-(cvds) (accessed 4.28.26).*
10. *Coagulation Cascade: Pathway and Clotting Steps | Osmosis [WWW Document], n.d. URL https://www.osmosis.org/answers/coagulation-cascade (accessed 4.28.26).*
11. *Dd, W., Ps, F., 2008. The vessel wall and its interactions. PubMed.*
12. *DETERMINATION OF AORTIC PRESSURE-TIME PROFILE, ALONG WITH AORTIC STIFFNESS AND PERIPHERAL RESISTANCE | Journal of Mechanics in Medicine and Biology [WWW Document], n.d. URL https://www.worldscientific.com/doi/abs/10.1142/S0219519404001193?journalCode=jmmb (accessed 4.28.26).*
13. *Disorders of blood viscosity - PubMed [WWW Document], n.d. URL https://pubmed.ncbi.nlm.nih.gov/8435185/ (accessed 4.28.26).*

14. *F, K., Dn, G., n.d. Compliant model of a coupled sequential coronary arterial bypass graft: effects of vessel wall elasticity and non-Newtonian rheology on blood flow regime and hemodynamic parameters distribution. PubMed.*
15. *G, T., Js, P., 2015. Inflammatory and immune responses in the arterial media. PubMed.*
16. *He, X., Luo, L.-S., 1997. Theory of the lattice Boltzmann method: From the Boltzmann equation to the lattice Boltzmann equation. Phys. Rev. E 56, 6811–6817. https://doi.org/10.1103/PhysRevE.56.6811*
17. *Hjm, B., Dw, T., Rb, H., Dl, S., Sj, P., Gg, F., Aj, F., Rn, R., Vc, H., Do, W., M, E., 1991. Beneficial effect of carotid endarterectomy in symptomatic patients with high-grade carotid stenosis. PubMed.*
18. *Hockney, R.W., n.d. Computer Simulation Using Particles.*
19. *I, B., U, L., 1982. Mechanism of the anticoagulant action of heparin. PubMed.*
20. *Jr, W., 1955. Method for the calculation of velocity, rate of flow and viscous drag in arteries when the pressure gradient is known. PubMed.*
21. *Jw, T., n.d. The Viscosity of Blood. PubMed.*
22. *K, N., R, K., J, T., Dm, S., R, D., Ja, L., Rs, B., K, O., Mj, B., n.d. Ethnic differences between extra-coronary measures on cardiac computed tomography: multi-ethnic study of atherosclerosis (MESA). PubMed.*
23. *Koschier, D., Bender, J., Solenthaler, B., Teschner, M., 2019. SPH Techniques for the Physics Based Simulation of Fluids and Solids.*
24. *Lindop, G., n.d. Diseases of blood vessels.*
25. *Monaghan, J.J., 1992. Smoothed Particle Hydrodynamics. https://doi.org/10.1146/annurev.aa.30.090192.002551*
26. *Mt, G., Jh, C., Rp, P., 2004. The biochemistry of nitric oxide, nitrite, and hemoglobin: role in blood flow regulation. PubMed.*
27. *Non-Newtonian Models | Materials | SimScale [WWW Document], n.d. URL https://www.simscale.com/docs/simulation-setup/materials/non-newtonian-models/ (accessed 4.28.26).*
28. *P. L. Bhatnagar, E. P. Gross, M. Krook, 1954. A Model for Collision Processes in Gases. I. Small Amplitude Processes in Charged and Neutral One-Component Systems | Phys. Rev. [WWW Document]. URL https://journals.aps.org/pr/abstract/10.1103/PhysRev.94.511 (accessed 4.28.26).*
29. *P, L., Je, B., L, B., Gk, H., J, D., Ms, B., L, T., Ef, L., 2019. Atherosclerosis. PubMed.*

30. *(PDF) Cardiovascular Mathematics [WWW Document], n.d. URL https://www.researchgate.net/publication/41517317_Cardiovascular_Mathematics (accessed 4.28.26).*
31. *Pedro Vayssiere Brandao, Pedro Vayssiere Brandao, Mohamed Najib Ouarzazi, Silvia C. Hirata, Antonio Barletta, 2004. (PDF) Darcy–Carreau–Yasuda rheological model and onset of inelastic non-Newtonian mixed convection in porous media [WWW Document]. URL https://www.researchgate.net/publication/351043454_Darcy-Carreau-Yasuda_rheological_model_and_onset_of_inelastic_non-Newtonian_mixed_convection_in_porous_media (accessed 4.28.26).*
32. *Pj, T., Mg, H., S, M., H, A., P, A., N, B., L, C., M, D., S, E., R, H.H., M, J., S, K., T, N., P, P., T, R., M, S., U, S., Jc, T., A, T., E, V., Ks, W., n.d. Mannheim carotid intima-media thickness and plaque consensus (2004-2006-2011). An update on behalf of the advisory board of the 3rd, 4th and 5th watching the risk symposia, at the 13th, 15th and 20th European Stroke Conferences, Mannheim, Germany, 2004, Brussels, Belgium, 2006, and Hamburg, Germany, 2011. PubMed.*
33. *Pollock, J.D., Makaryus, A.N., 2026. Physiology, Cardiac Cycle, in: StatPearls. StatPearls Publishing, Treasure Island (FL).*
34. *Robert H. Cole, 1948. Underwater Explosions. Princeton University Press.*
35. *S, M., 2018. The meaning of blood pressure. PubMed.*
36. *Sherwin, S.J., Blackburn, H.M., 2005. Three-dimensional instabilities and transition of steady and pulsatile axisymmetric stenotic flows. J. Fluid Mech. 533, 297–327. https://doi.org/10.1017/S0022112005004271*
37. *Tg, P., C, S., n.d. Vascular wall shear stress: basic principles and methods. PubMed.*
38. *Todd, B., 2005. Power-law exponents for the shear viscosity of non-Newtonian simple fluids. Physical review. E, Statistical, nonlinear, and soft matter physics 72, 041204. https://doi.org/10.1103/PhysRevE.72.041204*
39. *Tw, S., 2016. Hemodynamics. PubMed.*
40. *van de Vosse, F., Stergiopulos, N., 2011. Pulse Wave Propagation in the Arterial Tree. Annu Rev Fluid Mech 43, 467–499. https://doi.org/10.1146/annurev-fluid-122109-160730*
41. *Wang, X., Li, X., 2012. The influence of wall compliance on flow pattern in a curved artery exposed to a dynamic physiological environment: an elastic wall*

model versus a rigid wall model. J. Mech. Med. Biol. 12, 1250079. https://doi.org/10.1142/S0219519412005095

42. *Y, I., T, O., Y, S., T, Y., T, I., 2016. Numerical methods for simulating blood flow at macro, micro, and multi scales. PubMed.*
43. *Zhang, J., Xu, J., 2015. Rheological behaviour of oil and water emulsions and their flow characterization in horizontal pipes. The Canadian Journal of Chemical Engineering 94, n/a-n/a. https://doi.org/10.1002/cjce.22377*
44. *Zou, Q., He, X., 1997. On pressure and velocity boundary conditions for the lattice Boltzmann BGK model. Physics of Fluids 9, 1591–1598. https://doi.org/10.1063/1.869307*

Appendix

Appendix A: Vascular Anatomy

Blood from the arteries would be exchanged in the capillaries between the blood and tissue. The three types of capillaries are as follows. First, continuous capillaries which are present in most tissues, have tight junctions with intercellular clefts for water, irons, glucose, gases, and and hydrophobic molecules. In the brain they build up the blood-brain barrier. The second type is fenestrated capillaries, which are in the intestines, kidneys, choroid plexus, and endocrine glands, and contain pores that allow them to move larger molecules unlike the ones discussed earlier. Third and last are sinusoid capillaries that are located in the liver, spleen, bone marrow, and certain endocrine glands have large intercellular gaps and incomplete basement membrane, allowing for the passage of cells and plasma proteins.

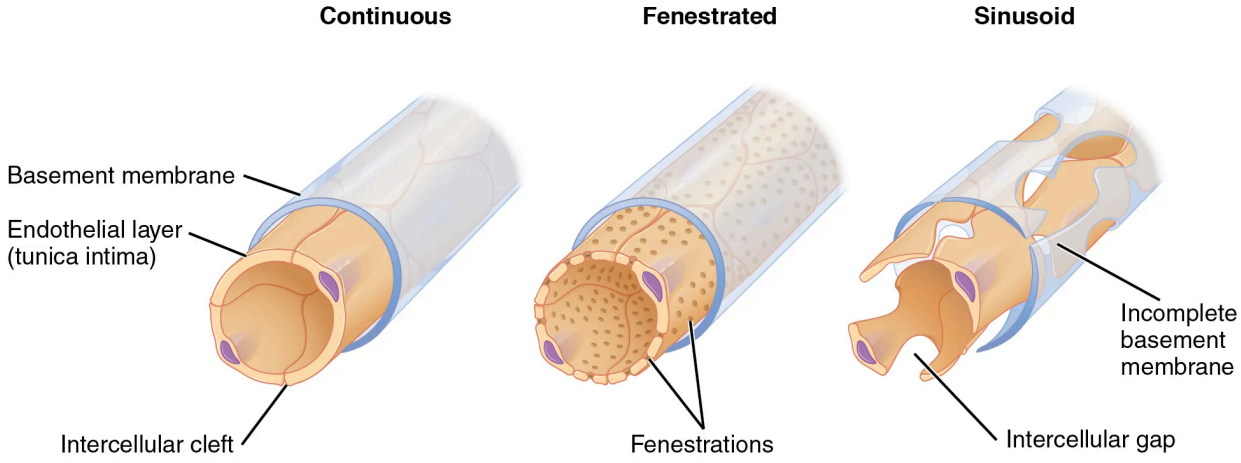

Capillary types figure

From the capillaries, the blood is collected by the venules, made up of an endothelium, a thin tunica media, and a thin tunica externa. Then, blood moves into the veins where they have thin walls, large lumens, and valves in between to ensure a unidirectional flow towards the heart, especially in the extremities where pressure is low and gravity opposes venous flow.

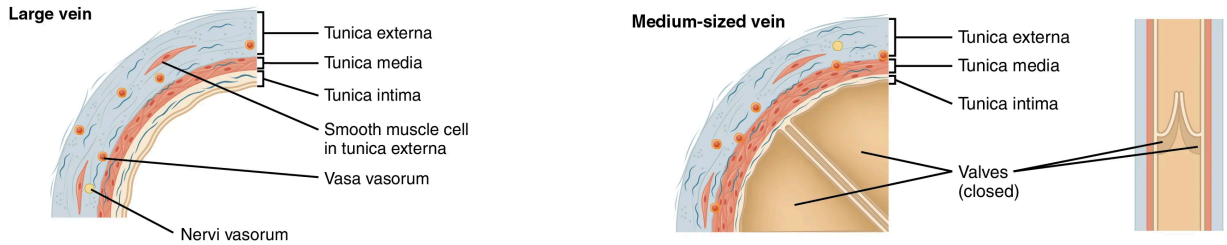

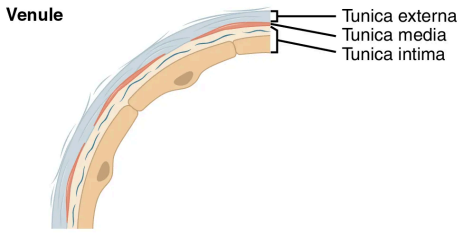

Vein types figure

Appendix B: Pathophysiology and Biochemical BG

Blood Composition and Cellular Elements

Blood is considered a connective tissue that is composed of approximately 55% plasma and 45% “formed elements”, such as **red blood cells (RBCs)**, **white blood cells (WBCs)**, and **platelets**.

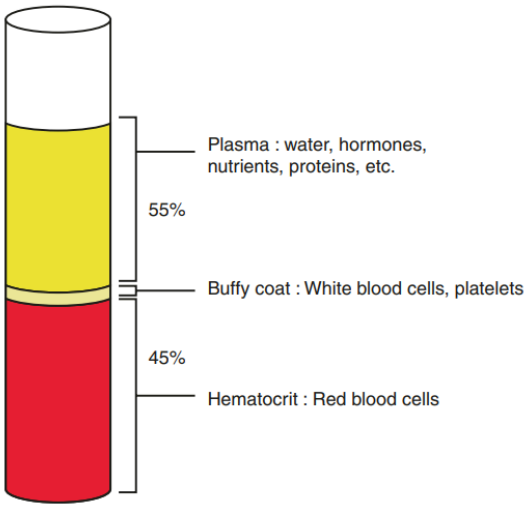

Plasma is approximately (could differ from individuals and contexts) 90% water, and its main purpose is to act as the main transporter through the cardiovascular system, transporting proteins (albumin, globulins, fibrinogen), electrolytes, hormones, and nutrients. The proteins within plasma have many uses, such as albumin, which maintains oncotic pressure, which is the osmotic pressure exerted by plasma proteins, that pulls water into the bloodstream from the tissue to maintain fluid balance. The second main protein that we talked about earlier is fibrinogen, which is produced in the liver and is part of the hemostasis process. Lastly are globulins that help in transporting proteins, enzyme inhibitors (alpha globulins), the transport of molecules such as lipoproteins and transferrin (beta globulin), and immunoglobulins (gamma globulins), which are antibodies.

RBCs are the most abundant in number, as biconcave disks that are filled with hemoglobin are used to transport O2 and CO2. WBCs (neutrophils, monocytes, lymphocytes, etc.) are in simple terms, the main anti-inflammatory and anti-body mechanisms of the body through phagocytosis, and tissue repair. Platelets help in hemostasis by forming the first layer/plug to coagulate any

wounds to prevent bleeding.

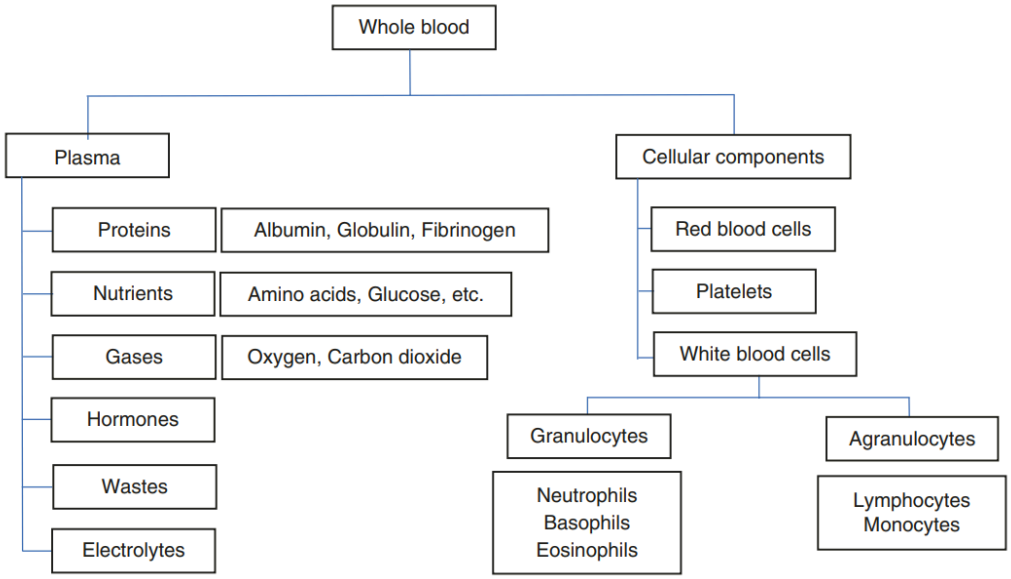

Components of blood figure

Cardiovascular Physiology and Anatomy

Having studied the background of the vascular structure and composition, it is important to shift from the vascular to the cardiovascular system, the heart. The cardiac cycle is multiple phases and events of mechanical and electrical changes in the heart during a single heartbeat, made of systole (contraction) and diastole (relaxation).

The atria and ventricles contract and relax inversely to move blood from the atria into the ventricles, and then into the pulmonary systemic circuits, and the diastole allows for the chambers to fill up again for the next contraction. Each chamber will go through four main phases:

- Filling
- Isovolumetric contraction
- Ejection
- Isovolumetric relaxation

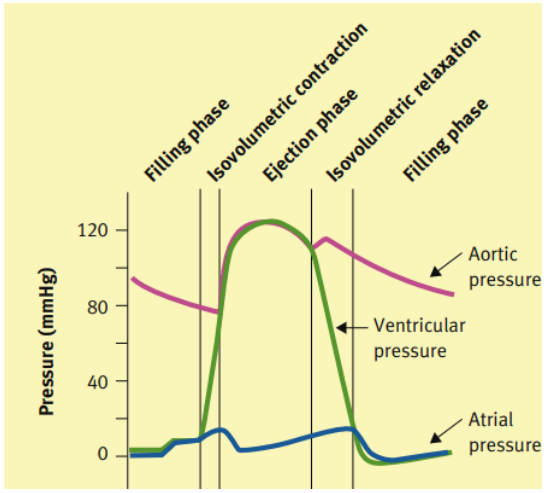

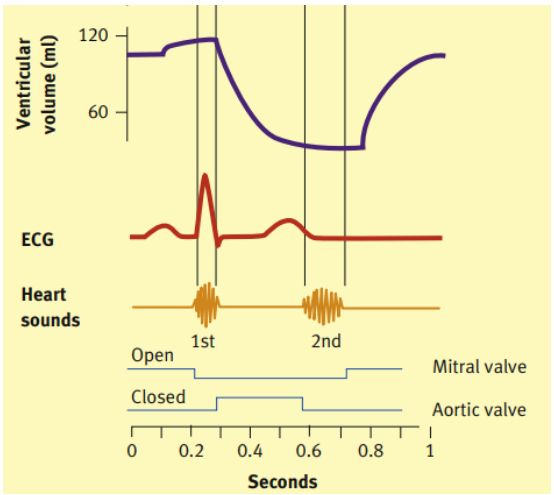

The heart is a four-chambered organ, with the atria as the receiving chambers, and ventricles as pumping chambers, both separated by the inter-atrial and inter-ventricular septa. Blood flow is controlled when to enter and leave by 4 main valves, the mitral (bicuspid, meaning two points), and tricuspid (three points) valves between atria and ventricles, and the aortic and pulmonary semilunar valves.

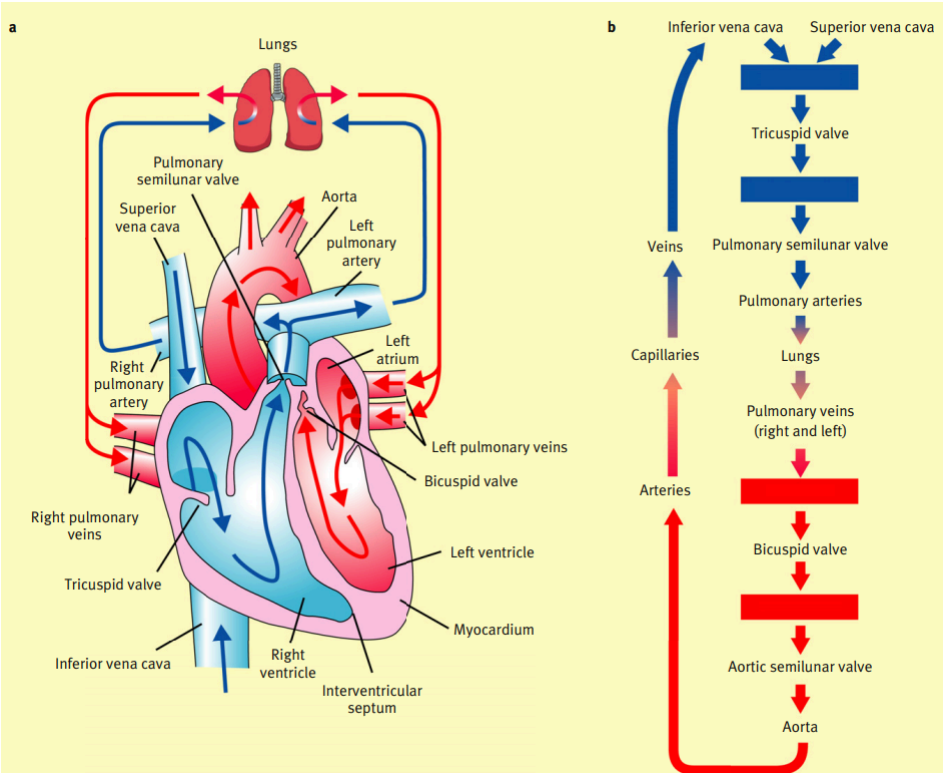

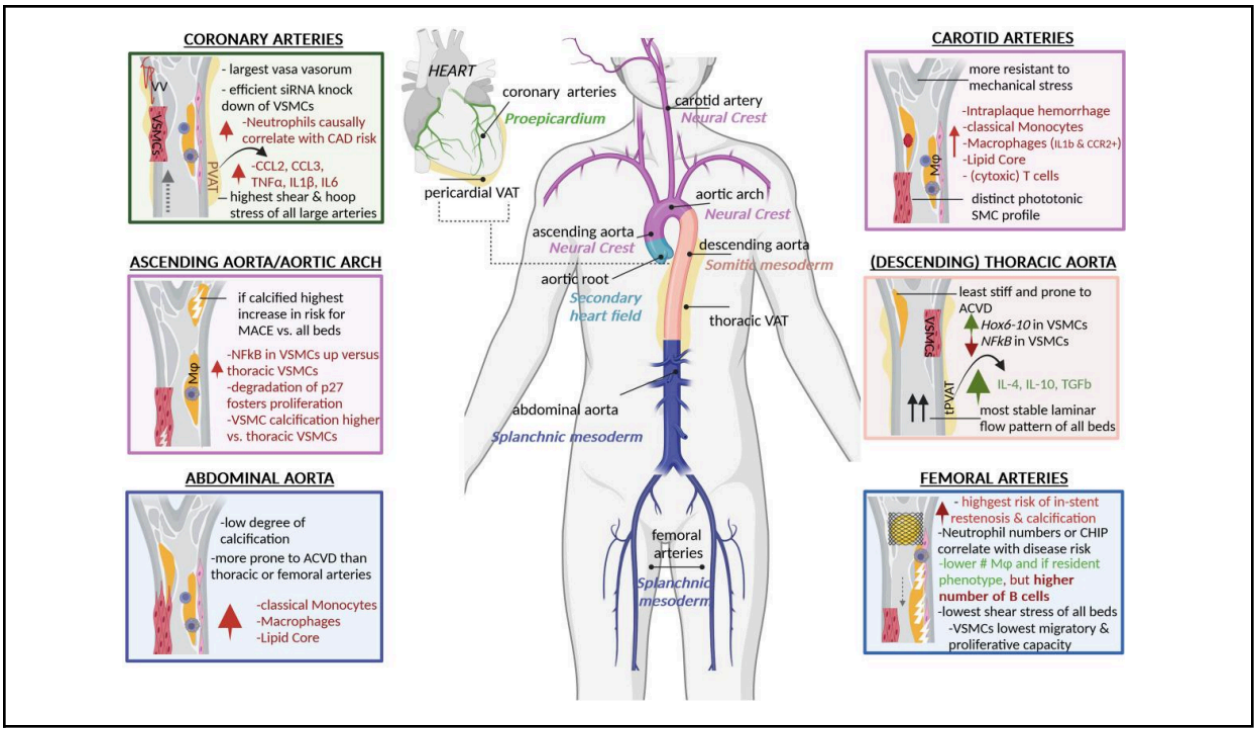

Vascular Smooth Muscle Cells (VSMC) and Embryonic Development

VSMC's, though run through the entire arterial system, differ in function and origins. The thoracic aorta VSMCs tend to have higher levels of $Hox6 - 10$ genes and reduced $NF - \kappa B$ activity, making them less prone to inflammatory activation. In contrast, VSMCs in the aortic arch, which originate from the neural crest during embryonic development have higher tendency towards calcification in comparison to somitic-derived VSMCs of the descending aorta. Femoral artery VSMCs tend to overexpress $TGF\beta R1$, increasing the chance of a phenotypic switch and mineral deposition, leading to the hemostatic and viscous environment of the lower limbs, which in turn explains heavy calcification commonly seen in femoral lesions despite their mesodermal origins during embryonic origins. These developmental changes at a molecular level explain why the:

- Carotid plaque tend to rupture
- Femoral plaque calcify
- Coronary plaques are highly inflammatoryCalcification and Mortality Across Different Vascular Beds

Vascular Bed Differences in Atherosclerotic Disease

Atherosclerosis does not behave uniformly throughout the arterial tree due to differences in biomechanics, flow patterns, different immune environments, and vascular smooth muscle cell (VSMC) behaviour.

The carotid artery is a major blood vessel on each side of the neck that supplies blood to the cephalic region (head). Plaque buildup is characterized by being more inflammatory. They contain mother densities of activated macrophages and metabolically active leukocytes, which can be seen using PET-CT imaging and single-cell RNA sequencing. These lesions typically show increased $IL - 1\beta$ positive macrophages, and an increased amount of $CCR2^{+}$that in turn increases leukocyte recruitment, and $CD8^{+}$ T cells. As such, the carotid environment allows for increased plaque buildup, more plaque rupturing, which will lead to an embolism or thrombosis in the cephalic region. These structural and inflammatory differences alter arterial stiffness, flow, and local shear stress, meaning they should be considered as assumptions that influence the boundary conditions and viscosity when simulating different regions in computational blood flow models.

The plaques in the femoral artery are mainly formed of foam-like cells and $TREM2^{+}$ macrophages, making it a more anti-inflammatory and homeostatic environment, the opposite of the carotid. Such plaques tend to calcify at higher rates, leading to sheet-like, nodular, and osteoid foreign bodies, but contain less cholesterol overall. This makes it a more stable and gradual progression, with a lower risk of a rupture, but increased chances of ischemia due to the narrow vessels, resulting in peripheral artery disease (PAD), which can progress to resting pain, then chronic ulcers, tissue necrosis, and gangrene of the lower limbs.

The coronary arteries are the blood vessels that wrap the heart's surface and deliver blood to the myocardium (heart muscles). Coronary arteries have the highest density of vasa vasorum (smaller vessels that feed arteries and veins), allowing for increased inflammatory infiltration and development of metabolically active, rupture-prone plaques.

Coronary VSMCs tend to migrate and proliferate at a higher capacity in comparison to femoral VSMCs, allowing for rapid plaque growth, accelerating restenosis following interventions such as an angioplasty or stenting. This behaviour in summary, explains the rather aggressive progression or coronary plaques, which lead to high rates of acute thrombosis.

Vascular Calcification and Mortality Rates

Arterial calcification correlates with mortality, but the rate of predication differs from different vascular regions, meaning each region does not carry the same prognostic weight, although it is universal of atherosclerosis. Large-scale studies comparing calcification of the thoracic aorta, abdominal aorta, carotids, iliac arteries, and coronary arteries have consistent patterns, where calcification in the thoracic aorta and carotid arteries shows a strong association with reduced survival.

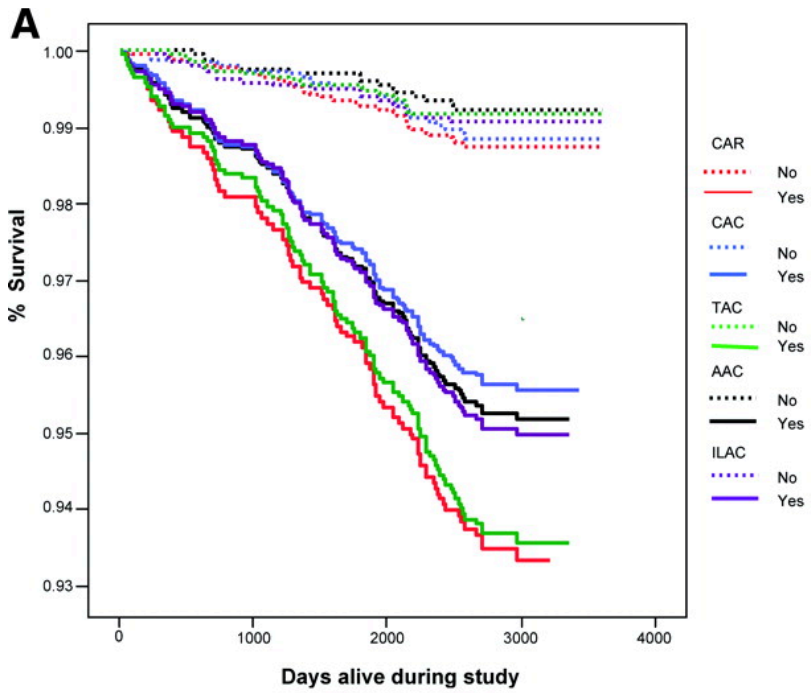

All-Mortality rate of Coronary (CAC), Thoracic Aorta (TAC), iliac (ILIAC), Carotid (CAR), Abdominal Aorta (AAC) figure

Those beds are highly elastic, so calcification here leads to “pulse-wave stiffness” and increased systolic pressure.

In contrast, coronary artery calcium (CAC), despite being the most widely used clinical scoring tool, shows the weakest separation between survival graphs.

The reason is not the fact that coronary calcification is benign, but rather that its pathophysiology meaning is different. First of all, coronary calcification means there is late-stage plaque stabilization, not plaque vulnerability. Second, the most dangerous coronary plaques are thin-cap fibroatheromas, which are non-calcified in most cases or at most minimally calcified. Lastly, the last two statements mean one thing: a patient with high CAC may have stable plaques, and a patient with low CAC may still have a small amount of dangerous unstable lesions.

This inverse relationship of high CAC but weaker mortality prediction happens because the coronary arteries are different from other beds. The coronary arteries have dense amounts of vasa vasorum, a metabolically active smooth muscle, and high rates of inflammation, meaning that non-calcified lipid-rich plaques have a higher risk. This coronary calcium is a great marker of total plaque, but not a weak one for plaque instability.

Chemical Regulation

Hemoglobin

Hemoglobin is a metalloprotein (a form of proteins that contain a heavy metal, such as iron, inside their chemical structure as a bond) required for oxygen transportation in the blood. It is built around the **Iron(II) heme group**, which allows for easy binding and release of oxygen.

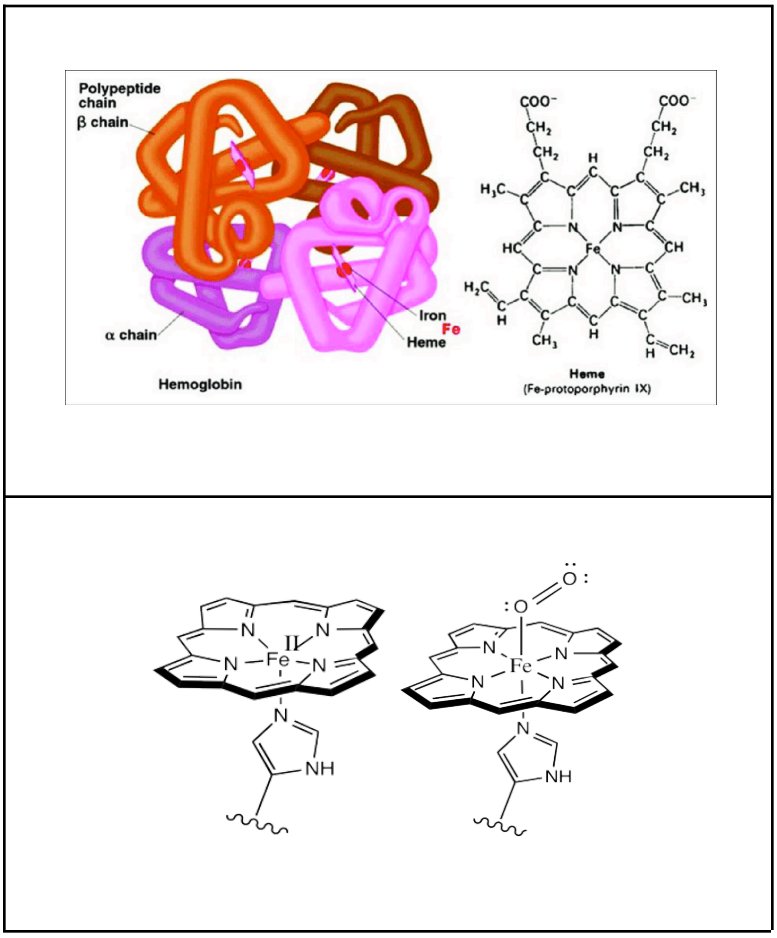

Figure 1: Deoxyhemoglobin and Oxyhemoglobin structure

(Chris Schaller, 2019)

The iron core of hemoglobin shifts in position relative to the heme group depending on if oxygen is present or not (note: oxygen does **not** react with the ferrous core, it only influences the structure without interacting on a chemical level). The shift can be summarized as the iron core being in a natural “dome” or “relaxed” structure when O_2 is not present, and “straightened” or “tense” structure when O_2 is present. In simple language, the Oxygen pulls on the ferrous particle, straightening the structure towards the porphyrin ring (the nitrogen-carbon ring around the core). Ultimately, this ability to shift structures in such a way allows for the almost perfectly reversible “reaction” (Chris Schaller 2019).

Vasoregulation and Nitric Oxide

In terms of vascular regulators, **Nitric Oxide (NO)** plays a major role in regulating vascular homeostasis. It is produced by the **endothelial Nitric Oxide Synthase (eNOS)** protein (Gladwin et al., 2004), using **L-arginine**, **NADPH**, oxygen, and hydrogen to produce the Nitric Oxide with some by products, such as **$NADP^+$** (low energy state of NADPH). The exact formula looks like this:

$$2\,L\_arginine + 3\,NADPH + 4\,O2 + H(+) = 2\,L\_citrulline + 2\,nitric\,oxide + 3\,NADP(+) + 4\,H2O$$

[Expasy (NA)]

Additionally, hemoglobin can function as a nitrite reductase, allowing for the generation of NO in **hypoxic conditions**. The deoxygenated Hb reduces the nitrite into NO through the following reaction (Gladwin et al., 2003):

$$NO_2^- + HbFe^{2+} + H^+ \rightarrow HbFe^{3+} + NO^+$$

$$NO + HbFe^{2+} \rightarrow HbFe^{2+}NO$$

This connects oxyhemoglobin to NO production, acting as a natural NO detector/sensor (Gladwin et al., 2003).

Coagulation & Anticoagulation Mechanisms

Moving onwards, we have **coagulation** and **anticoagulation mechanisms**. Coagulation works in a **cascade** (primary, which makes a weak, temporary clot, and secondary, which makes a stronger, more permanent clot) that is split into three main parts, with the first two being responsible for activating the **clotting factor X** (such will be used later in the formation of the clot itself) (De Caterina et al. 2013):

Extrinsic Pathway: This pathway is initiated by **Tissue Factor III** (only the number will be used for referral), which is “released” into the bloodstream when cells are damaged. This also activates it into **IIIa**, which will be used later on in the common pathway. Additionally, **Tissue Factor VII** is released and activated, making **VIIa**.

- The extrinsic pathway is more fast acting, but leads to a weaker clot later in the common factor.

Intrinsic Pathway: This pathway is initiated by the **collagen** (from damage to subendothelial/endothelial tissue), **kallikrein** (from blood vessel damage), and **high molecular weight kininogen (HMWK)** factors (generally found in blood plasma, but plays a role here). These proteins activate the **Hageman factor XII** into **XIIa**. XIIa activates **XI** into **XIa**, and, with some calcium^{+2}, XIa activates **IX** into **IXa**. Simultaneously, during these activations, factor **VIII** is

activated into **VIIa** with some **thrombin** (i.e., **factor IIa**), which is then used with factor XIa and calcium^{+2} later in the **Common Pathway**.

- The intrinsic pathway is slower than the extrinsic, but it “amplifies” the clots’ strength.

Common Pathway: Using the activated factors XIa and VIIa with some calcium^{+2}, coagulation factors X get activated into Xa. On a side cascade under this, factor V with some pre-existing thrombin (IIa) present in the blood even without the injury activates Va. The activated Va is then used with the Xa and some calcium^{+2} to then activate even more thrombin (II → IIa). With the increased thrombin content present (and the inhibited anti-coagulants), **fibrinogen** (factor I) is activated into **fibrin** (Ia). The fibrin, with the stabilizing factor **XIIIa** (XIII + Thrombin → XIIIa), and some calcium^{+2}, **finally creating a stable clot** (Corinne, 2025).

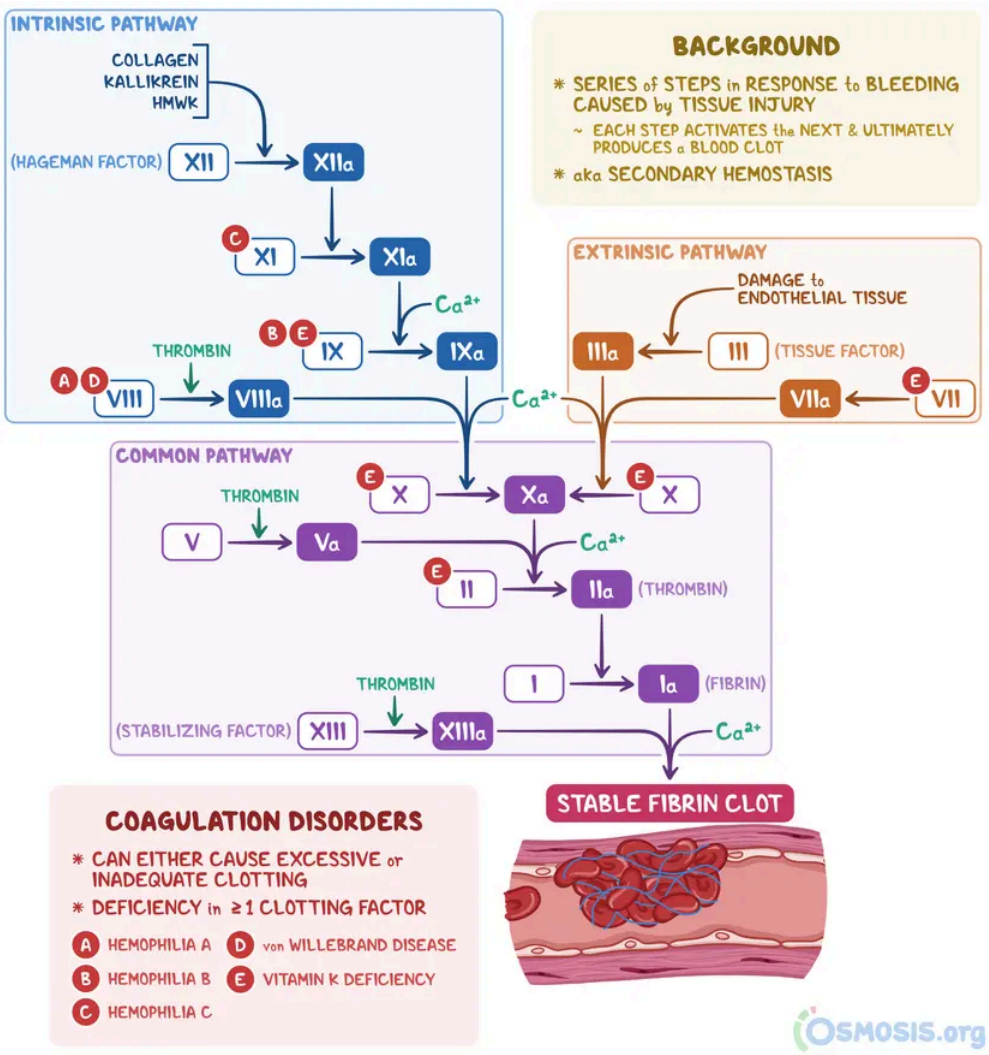

(Corinne, 2025) figure

In short, the extrinsic and intrinsic pathways create the necessary complexes needed to activate factor X, which is used to synthesize fibrin to form the clot (platelets are also involved in the clot creation process, but for the sake of our scope, they will not be mentioned.)

However, the common pathway is often inhibited unless needed to stop the blood thrombin levels from climbing too high. This is done so by the **anticoagulation mechanisms**. Only **Antithrombin (AT)** will be explored here, however.

Thrombin is always present in the blood in very miniscule quantities, with that being the case because of AT inhibiting the thrombin from cleaving other proteins and initiating the feedback loop. AT is in function a **serine protease inhibitor** (the activated coagulation factors from earlier are under the category of “serine proteases”. They cleave other proteins’ peptide bonds), neutralizing thrombin and other coagulation enzymes (Xa, IXa, XIa, XIIa) by forming an irreversible complex completely halting the enzyme’s catalytic activity (in simple words: it locks the activated factor from working permanently) (Rosenberg et al. 1984).

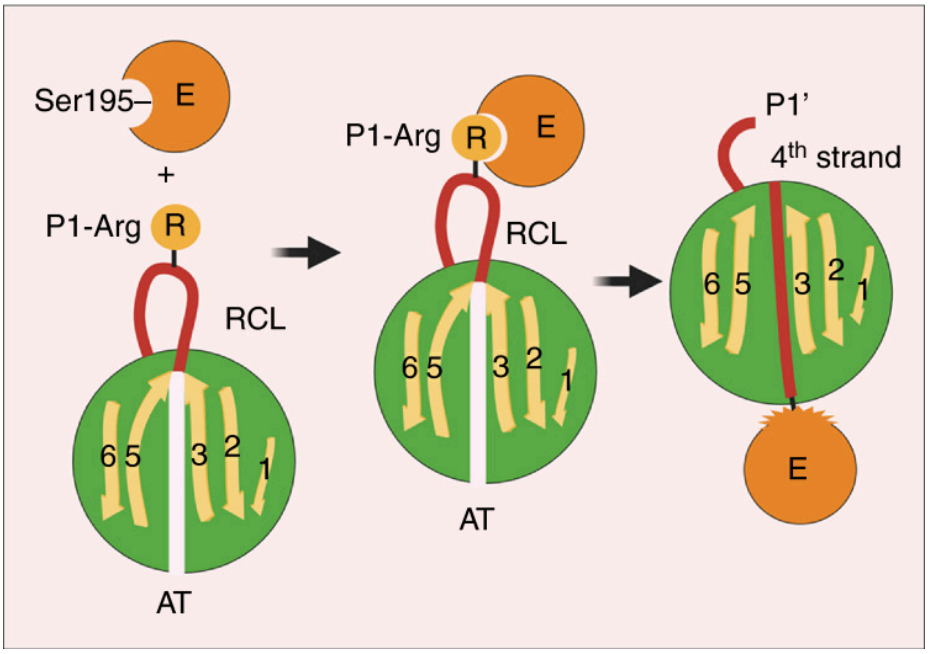

(Bird et al., 1987) figure

The figure here shows how a coagulation factor would interact with the antithrombin’s reactive site (the strand), creating a covalent bond between the two. The coagulation factor would then cleave at the reactive site, triggering the insertion of the reactive loop into **β-sheet A**. This creates a large conformational change in the antithrombin, effectively “pulling” the coagulation factor violently and thereby destroying its functionality (Bird et al., 1987).

This inhibition is often accelerated via **heparin**, specifically heparan sulphate, the naturally occurring form in the human body. Heparan sulphate binds with the antithrombin molecule itself,

exposing it into a more optimal position. This binding also induces a conformational change in the antithrombin, causing it to be more **rigid**, and consequently, more capable of destroying the coagulation factors. Moreover, the now bound heparan sulphate causes a “bridging” effect between the antithrombin and thrombin/factor Xa (think the heparan “pulling” the factors closer to the antithrombin), increasing their local concentrations and thereby the reaction rates (Björk and Lindahl, 1982).

Electrolytes and Blood Chemistry

Blood chemistry and behaviour is highly reliant and sensitive to the access of electrolytes and other chemicals (both biotic and abiotic). In terms of the electrolytes, the main forms would be **potassium (K^+)**, **sodium (Na^+)**, **calcium (Ca^{2+})**, **magnesium (Mg^{2+})**, **bicarbonate (HCO_3^-)**, and **chloride (Cl^-)**. Electrolytes regulate and allow bodily functions, such as maintaining fluid balance, support muscle and nerve function, **regulate heart rhythm** (more so with the sodium, potassium, magnesium, and calcium), and help control blood pH. Similarly, proteins, such as **albumin** and other blood proteins, are essential for nutrient transport, maintaining osmotic pressure (albumin plays a more major role here. Likewise with nutrient transport with it being the main “carrier” of such), and supporting the overall metabolic health of the body (Hirsch, 2023).

Focusing on electrolyte impact on vascular health, potassium and sodium levels (only these two will be explored) influence the contractile behaviour (ability to contract and relax) of vascular smooth muscle (arteries); increasing extracellular potassium in large vessels (0–24 mM) raised intracellular potassium levels, boosting contractility and relaxation rates, improving function.

In a similar regard, these same electrolytes can work as both inhibitors and stimulants to certain functions and/or reactions. For example, moderate increases (to 10 mM) reduced epinephrine-induced contraction, while higher levels (24 mM) enhanced it. Similarly, higher Na^+ reduced the smooth muscle’s responsiveness to epinephrine while lower levels “potentiated it” (stimulated it) (David F., 1961).

Note: Without going too deep, epinephrine constricts the vessels by binding to an α_1 receptor, telling most smooth muscle to constrict, while **dilating** some via the β_2 receptor. While the α_1 is present in most sections of the body, the β_2 is present predominantly in heart and musculoskeletal vessels. In other words, the fight or flight response.

Appendix C Mathematical Derivations

Derivations

Two-element Windkessel Model derivation

Here, we are deriving the two element Windkessel model from the conservation of volume and the relationship:

$$\frac{dP}{dt} = \frac{dP}{dV} \cdot \frac{dV}{dt} = m\frac{dV}{dt},$$

To start the derivation, we will need some terms will need to be “expanded” to continue with this:

The outflow rate $Q(t)$ can be expressed as:

$$Q(t) = \frac{P(t)}{R},$$

In hemodynamics, flow through a resistance R (viscosity, friction, drag, etc.) is proportional to the pressure difference $P(t)$ (also known as Ohm’s Law analogy). Moving forward with this new form, we can substitute it back into the original conservation of volume equation we had earlier, which gives us:

$$\frac{dV}{dt} = I(t) - \frac{P(t)}{R}.$$

Returning back to the inverse of compliance, we can derive it by first describing compliance, which is expressed as:

$$C = \frac{dV}{dP},$$

This would be the nonlinear form of the equation (and the otherwise “typical” form). To properly link it, and consequently simplifying it, we can **linearize** the equation by assuming that the compliance is constant, giving us:

$$V = V_0 + CP,$$

Where the initial volume V_0 would be the “unstressed” volume before applying any pressure.

This form can allow us to take the **time derivative**, returning us to the relationship from earlier:

$$\frac{dV}{dt} = C\frac{dP}{dt},$$

Isolating for $\frac{dP}{dt}$, we get:

$$\frac{dP}{dt} = \frac{1}{C}\frac{dV}{dt}$$

And as we stated earlier, the inverse of compliance is just m, “reducing” this into the earlier relationship perfectly:

$$\frac{dP}{dt} = m\frac{dV}{dt}$$

And since we've proven that $\frac{dV}{dt}$ equals to $I(t) - \frac{P(t)}{R}$, we can substitute this into the relationship here, giving us:

$$\frac{dP}{dt} = m\left(I(t) - \frac{P(t)}{R}\right),$$

Expanding this:

$$\frac{dP}{dt} = mI(t) - \frac{m}{R}P(t)$$

And making the $mI(t)$ term the subject of the formula should give us:

$$\frac{dP}{dt} + \frac{m}{R}P(t) = mI(t)$$

In paper:

Relationship

$$\boxed{\frac{dP}{dt} = \frac{dP}{dV} \times \frac{dV}{dt} = m\frac{dV}{dt}}$$

Conservation of Volume:

$$\frac{dV}{dt} = I(t) - Q(t)$$

Outflow:

$$Q(t) = \frac{P(t)}{R}$$

$$m = \frac{1}{C}$$

Substituting =

$$\frac{dV}{dt} = I(t) - \frac{P(t)}{R}$$

Substitute $\frac{dP}{dt} = m\frac{dV}{dt}$

$$\frac{dP}{dt} = m\left[I(t) - \frac{P(t)}{R}\right]$$

$$\frac{dP}{dt} = mI(t) - \frac{m}{R}P(t)$$

take the time derivative

$$\frac{dV}{dt} = C\frac{dP}{dt}$$

Isolating for $\frac{dP}{dt}$

$$\frac{dP}{dt} = \frac{1}{C}\frac{dV}{dt} \rightarrow \boxed{\frac{dP}{dt} = m\frac{dV}{dt}}$$

Isolate for $mI(t)$:

$$\frac{dP}{dt} + \frac{m}{R}P(t) = mI(t)$$

target equation

$$\boxed{\frac{dP}{dt} + \frac{m}{R}P(t) = mI(t)}$$

Compliance Equation

$$C = \frac{dV}{dP}$$

Linearize the equation

$$\boxed{V = V_0 + CP}$$

Integration of the Basic Inflow Equation

Working out the integration:

Integration of $I(t) = ae^{-bt}t(t_s - t)$

$$\int ae^{-bt}t(t_s - t)\,dt$$

treat all vars not "t" as constant

$$a\int e^{-bt}t(t_s - t)\,dt$$

expand =

power rule $\int x^n dx = \frac{x^{n+1}}{n+1} + c$

$$a\int e^{-bt}(tt_s - t^2)\,dt$$

$$a\left(\int e^{-bt}t_s t\,dt - \int e^{-bt}t^2\,dt\right)$$

$\int u\,dv = uv - \int v\,du$

$u = t \quad du = 1\times dt$

$v = \frac{e^{-bt}}{-b} \quad dv = e^{-bt}dt$

$$a\left(t_s\int e^{-bt}t\,dt - \int -t^2e^{-bt}\,dt\right)$$

$u = t^2 \quad du = 2t\,dt$

$v = \frac{e^{-bt}}{-b} \quad dv = e^{-bt}$

$$a\left(t_s\left(t\times\frac{e^{-bt}}{-b} - \int\frac{e^{-bt}}{-b}\,dt\right) - \left(t^2\frac{e^{-bt}}{-b} + \int\left(\frac{e^{-bt}}{-b}\right)(2t)\,dt\right)\right)$$

$u = t \quad du = 1\,dt$

$v = \frac{e^{-bt}}{-b} \quad dv = e^{-bt}dt$

$\int -\frac{1}{b}e^{-bt}\,2t\,dt \qquad -\frac{2}{b}\int e^{-bt}t\,dt$

$v \quad u$

$$a\left(t_s\left(-\frac{t}{b}e^{-bt} - \frac{1}{b^2}e^{-bt}\right) - \left(-\frac{t^2}{b}e^{-bt} + \frac{2}{b}\left(-\frac{t}{b}e^{-bt} - \frac{1}{b^2}e^{-bt}\right)\right)\right)$$

$$a\left(t_s - e^{-bt}\left(\frac{t}{b} + \frac{1}{b^2}\right) - \left(-\frac{t^2}{b}e^{-bt} - \frac{2t}{b^2}e^{-bt} - \frac{2}{b^3}e^{-bt}\right)\right)$$

$$a\left(t_s - e^{-bt}\left(\frac{t}{b} + \frac{1}{b^2}\right) - \left(-e^{-bt}\left(\frac{t^2}{b} + \frac{2t}{b^2} + \frac{2}{b^3}\right)\right)\right)$$

$$a\left(t_s - e^{-bt}\left(\frac{t}{b} + \frac{1}{b^2}\right) - \left(-e^{-bt}\left(\frac{t^2}{b} + \frac{2t}{b^2} + \frac{2}{b^3}\right)\right)\right)$$

factor out the $-e^{-bt}$

$$a\left[-e^{-bt}\right]\left(t_s\left(\frac{t}{b} + \frac{1}{b^2}\right) - \left(\frac{t^2}{b} + \frac{2t}{b^2} + \frac{2}{b3}\right)\right)$$

distribute the negative

$$ae^{-bt}\left(-t_s\left(\frac{t}{b} + \frac{1}{b^2}\right) + \left(\frac{t^2}{b} + \frac{2t}{b^2} + \frac{2}{b3}\right)\right)$$

expand

$$ae^{-bt}\left(-\frac{t_s t}{b} - \frac{t_s}{b^2} + \frac{t^2}{b} + \frac{2t}{b^2} + \frac{2}{b^3}\right)$$

group

quadratic $\frac{t^2}{b}$

Linear $-\frac{t_s t}{b} + \frac{2t}{b^2}$

$t\left(-\frac{t_s}{b} + \frac{2}{b^2}\right)$

constants $\frac{t_s}{b^2} + \frac{2}{b^3}$

$\frac{1}{b}\left(\frac{t_s}{b} + \frac{2}{b^2}\right)$

$$ae^{-bt}\left(\frac{t^2}{b} + t\left(\frac{t_s}{b} - \frac{2}{b^2}\right) + \frac{1}{b}\left(\frac{t_s}{b} + \frac{2}{b^2}\right)\right) + C$$

factoring $\frac{1}{b}$ out of the expression

$$ae^{-bt} \cdot \frac{1}{b}\left(t^2 + t\left(t_s - \frac{2}{b}\right) + \left(t_s + \frac{2}{b}\right)\frac{1}{b}\right) + C$$

$$\therefore \frac{a}{b}e^{-bt}\left(t^2 + t\left(t_s - \frac{2}{b}\right) + \frac{1}{b}\left(t_s + \frac{2}{b}\right)\right) + C$$

which adhers with the final equation provided by Zhong et al. (2004)

With integration of Eq. (6) with respect to time, we can formulate the LV volume ejected into the aorta (or blood volume input into the aorta) during the systolic phase, as:

$$V = \frac{a}{b}e^{-bt}\left[t^2 + t\left(\frac{2}{b} - t_s\right) + \frac{2/b - t_s}{b}\right] + \text{constant}. \quad (7)$$

Zhong et al. (2004)

Lattice Boltzmann Method (LBM)

The Lattice Boltzmann Method (LBM), originating from Boltzmann's gas automata, is a mesoscopic computational fluid dynamics method that is used to simulate fluid flow by tracking the "evolution" of particles that are distributed over a discrete lattice, thus the name. Unlike most CFD solvers where it solve macroscopic equations (Navier-Stokes) directly, rather the LBM models fictive fluid particles that then propagate and collide on other lattice nodes, then macroscopic properties such as velocity or density is recovered as moments of these distributions.

The basic LBM evolution equation is defined with the BGK (Bhatnagar-Gross-Krook) collision approximation as the following:

$$f_i(X + e_i\delta t, t + \delta t) = f_i(x, t) + \frac{f^{eq}{}_i(x,t) - f_i(x,t)}{\tau_f}$$

Where f_i

Smoothed Particle Hydrodynamics (SPH)

Smoothed particle hydrodynamics (or SPH for short) is a Lagrangian numerical method used to solve the governing equations of fluid dynamics (e.g. Navier-Stokes equations or Euler's equations) by discretizing the fluid into a set of moving particles (separating the fluid into multiple fluid parcels). Like any Lagrangian fluid solver, SPH is **freemesh**, not needing a grid to govern the movement of the fluid parcels. Unlike other solves, SPH **approximates** any field quantity $A(r)$ by a **weighted interpolation** over neighbouring particles using a **smoothed kernel** usually defined as $W(|r_i - r_j|, h)$. In the simplest of conditions, the SPH method is defined as:

$$A(r) \approx \sum_j V_j A(r) W(|r_i - r_j|, h)$$

Eq. (27)

Where V_j is the volume associated to the particle j. The smoothing kernel governs how much neighbouring particles can influence the selected particle, such increases with proximity

(subtracting the distance difference between our selected particle from our neighbouring particle. Smaller values mean bigger influences). h is the smoothing length.

Upon this system, there are some governing equations (in continuum form) that define how the fluid should behave:

Continuity (conservation of mass)

$$\frac{d\rho}{dt} = -\ \rho\nabla \cdot v$$

Eq. (28)

Momentum (Euler/Navier-Stokes. No viscosity)

$$\frac{dv}{dt} = -\ \frac{1}{\rho}\nabla p\ +\ g$$

Eq. (29)

Equation of state (to "close the system". Used in weakly compressible systems)

$$p\ = c^2(\rho\ -\ \rho_0)$$

Eq. (30)

Where ρ is the density, ρ_0 is the rest density, g is gravity, p is pressure, c is the numerical speed of sound, ∇ denotes the gradient operator (divergence; positive means "expansion", negative means "compression" towards points).

However, since these equations are that for continuum systems, they are discretized under SPH, giving us these forms for the continuity and momentum equations:

Density Summation:

$$\rho_i = \sum_j m_j W(|r_i - r_j|,\ h)$$

Momentum Equation:

$$\frac{dv_i}{dt} = -\sum_j m_j\left(\frac{p_i}{\rho_i^2} + \frac{p_j}{\rho_j^2}\right)\nabla W_{ij}\ +\ g$$

Where ∇W_{ij} is the gradient of the smoothing kernel. In simple terms, it states how differences in the position of particle i will change the influence of particle j and in what direction. So if particle i were to move a distance to the right, the gradient should tell us how the original influence of particle j has now changed and in what direction it is now pointing at.